Transportation Research Part C 132 (2021) 103385

Contents lists available at ScienceDirect

Transportation Research Part C

journal homepage: www.elsevier.com/locate/trc

Terminal area control rules and eVTOL adaptive scheduling model for multi-vertiport system in urban air Mobility

Quan Shao [a,1,*], Mengxue Shao [a,1], Yang Lu [b]

[a] College of Civil Aviation, Nanjing University of Aeronautics and Astronautics, Nanjing 211100, China
[b] College of Aerospace Engineering, Nanjing University of Aeronautics and Astronautics, Nanjing 211100, China

ARTICLE INFO

Keyword:
Urban air mobility
eVTOL
Adaptive control system
Operational structure
Scheduling model
Multi-vertiport system

ABSTRACT

On the one hand, vertiports in economically developed areas will present the operation mode of multi-vertiport, and the contradiction between the development of urban air mobility and limited operating resources is very serious. On the other hand, unlike fixed-wing aircraft or helicopters, the electric vertical take-off and landing (eVTOL) aircraft have different operating processes and limited battery energy supply. Long flight times in the terminal area pose a risk of exhaustion and great safety challenges. Given the terminal area of the multi-vertiport system (MVS-TA), this paper investigates the adaptive control system (ACS), which includes the design of the operating environment and the integrated scheduling model. The design of the operating environment is the basis of adaptive management, which consists of the concept of multi-ring structure and the junction control rules based on backpressure policy. Considering the power constraint and dynamic priority, an integrated model including path planning model and distributed sequencing model is constructed to solve the cooperative scheduling problem of approach-departure flights. Results from numerical analyses reveal that: First, in the case of large flight flow, ACS can achieve the efficiency and safety of MVS-TA operation better than the traditional control system. Secondly, the flight density into the terminal area has a greater impact on ACS performance relative to flight volume. With a density of less than 120 flights/hour, the operating efficiency of MVS-TA under ACS varies within 10.3% with the number of flights or density.

1. Introduction

1.1. Background

The commercial Urban Air Mobility (UAM) operations can be traced back to the United States in the 1840s (Pradeep, 2019). For example, Las Vegas Airlines and New York Airlines are used to transport people and mail between several locations. Although the operation of UAM was gradually terminated in the 1880s (Pradeep, 2019) due to accidents caused by mechanical failure, there is still a demand for commercial UAM operations to avoid transportation congestion on the ground.

However, current aviation technologies have reached a level of maturity to enable UAM to use quiet and efficient vehicles to conduct on-demand and scheduled operations (Thipphavong et al., 2018). UAM is a new type of urban low-altitude transportation

* Corresponding authors.
E-mail address: shaoquan@nuaa.edu.cn (Q. Shao).
[1] Quan Shao and Mengxue Shao are co-first authors of the article.

https://doi.org/10.1016/j.trc.2021.103385
Received 12 October 2020; Received in revised form 6 September 2021; Accepted 8 September 2021
Available online 22 September 2021

application, which uses a small all-electric or hybrid-electric vertical take-off and landing vehicle (VTOL) as the main means of transport to provide sustainable and affordable passenger or cargo transport services (Li et al., 2020; Thipphavong et al., 2018). Electric Vertical Take-Off and Landing (eVTOL) aircraft integrates advanced autonomous flight and distributed power technology. Complementing the traditional rotorcraft with longer voyages, eVTOL will be mainly used for short-air transportation services in urban areas. Its potential markets include, but are not limited to, passenger transportation services (such as air taxis, shuttle services), cargo services (German et al., 2018), medical rescue, public safety (Thipphavong et al., 2018), etc.

The key issues in the development of UAM include automated flight and contingency management, airspace system design, community integration, distributed power systems, reliability, etc. (Littell, 2019; Thipphavong et al., 2018; Vascik and Hansman, 2018). From the point of view of airspace structure design and operation management, this paper studies the efficient operation of the UAM terminal area. Due to UAM's mission positioning and application needs, the economically developed and densely populated metropolitan area will certainly have the trend of vertiport-intensive distribution, two or more vertiports in a certain area of co-operation, involving the sharing and competition of space–time resources between multiple vertiports, that is, the "Multi-vertiport System (MVS)" development mode. The operation control problem of the MVS-TA is one of the important links in the airspace management system, which focuses on how to design the route structure, operating rules, and control strategy to adapt to the operation characteristics of high density and high traffic in the terminal area and the power limit of eVTOL.

The existing air traffic management means are relatively ineffective. First of all, eVTOL has different operational processes and limited power, and the types of aircraft targeted by traditional civil aviation or general aviation air traffic control methods are completely different. Inefficient and cumbersome scheduling can cause flights to delay too long, creating the risk of running out of power and great safety challenges. Second, UAM's main operating airspace is concentrated in Class E, Class G airspace, or low airspace below 1000 m (inclusive) (Thipphavong et al., 2018). High-density traffic environments, urban airspace environments, and conflict resolution can greatly increase the complexity of scheduling strategies. The traditional scheduling method is based on flight planning or deterministic operating environment, obviously cannot effectively solve the MVS-TA flight scheduling problem. Even the UAS Traffic Management Framework (UTM) being built by countries (Prevot et al., 2016) is only for small unmanned aerial vehicles in airspace below 120 m, which can neither cover the airspace of UAM nor fully meet the management needs of MVS (Mohamed Salleh et al., 2017).

1.2. Literature review

The study of airspace structure in the UAM terminal area is usually combined with flight scheduling. (Bertram and Wei, 2020) proposes an airspace design of a terminal area containing boundaries and several centric rings. Markov Decision Model (MDP) is used to schedule flights around the ring layer. use the to guide the operation of flights. (Kleinbekman et al., 2018) initially designed the route structure with multiple arrival fixes/routes. Drawing on the concept of dynamic geofencing in UTM, (Zhu and Wei, 2019) proposes a conflict-free route pre-planning method to achieve on-demand occupancy of airspace, based on which a pre-planning algorithm for departure flight trajectories based on two-stage optimization is constructed.

In terms of urban airspace route structure design, the Metroplis team proposed the concept of unstructured airspace (Full Mix) operation and three types of structured airspace (Layers, Zones, Tubes). Comparing the four urban airspace structures from the perspectives of traffic density, complexity, and robustness, (Vidosavljevic et al., 2015) considered that Layers have a good balance between completely unstructured concepts and structured concepts, which is the best concept of complexity. Since there are many conflicts and intrusions in each concept, (Sunil et al., 2016) recommends investigating novel conflict detection and resolution algorithms that cope with the limited maneuvering room available at extreme traffic densities. To meet eVTOL's need for dynamic changes in urban airspace, (Mohammed Salleh et al., 2018) has planned three route structures for UAM: route network in AirMatrix, route network over buildings, and route network over Roads, and evaluates the performance in terms of capacity and throughput. The AirMatrix-based route can meet the needs of larger airspace capacity and traffic throughput, but it requires a highly automated and robust UAM management system for unified scheduling.

For on-demand features of UAM flights, (Pradeep, 2019) proposes the concept of Required Times of Arrival (RTA) to schedule approach flights. The study used Mixed-integer Linear Programming (MILP) models and Time-advance (TA) strategies to schedule RTAs for flights to reduce their air waiting times in the terminal area. Further to the approach process, (Pradeep, 2019) and (Pradeep and Wei, 2018) put forward the method of absorbing delay by optimizing speed and Shallow Descent flight, respectively, to obtain the energy-saving trajectory with the assigned RTA. Based on MILP and shallow descent control, the approach sequence satisfying RTA is calculated under the limits of residual battery power and vertiport capacity, but the system can only effectively handle the scheduling of 40 flights at most at frequency of 40 arrivals/hr (Kleinbekman et al., 2018). Expanding the research problem to the double-vertipad vertiport, (Kleinbekman et al., 2020) builds a rolling-horizon scheduling model that optimizes the average delay time of eVTOL to 50 s of the RTA. Besides, (Brittain and Wei, 2018)applied a hierarchical deep reinforcement learning framework to the sequencing and interval management of approaching flights. However, the robustness of artificial intelligence methods applied to air traffic management needs to be further improved.

In the control of UAM operation process, (Bosson and Lauderdale, 2018) presents an initial implementation of autonomous network management and aircraft separation service, and analyzes the impact of space interval, time interval and arrival scheduling horizon on delay time and conflict resolution. To achieve eVTOL conflict-avoidance and autonomous flight, the methods used at present include Markov Decision Model (MDP) (Bertram and Wei, 2020; Yang et al., 2019), autonomous network management and separation services (Bosson and Lauderdale, 2018), pre-flight planning based on dynamic geofence(Zhu and Wei, 2019), etc.

Overall, the multi-faceted study of UAM terminal area is of great reference significance, but there are still the following problems **1)**

The study of the airspace structure of the terminal area is usually limited to the concept of simple route structure, which is difficult to cope with the operation of UAM high-traffic high-density flights, and cannot improve the efficiency of flight operation from the mechanism. **2)** The flight scheduling in the terminal area is limited to the optimization of approach or departure of a single, and the process of approach and departure is completely stripped off. MVS has the characteristics of many components, complex airspace structure and large flight flow, not a simple composite of a single vertiport. Existing research cannot achieve MVS resource coordination and integrated optimization. **3)** At this stage, the conflict avoidance study is not combined with the design of the airspace structure of the terminal area. In the mature stage of UAM, which is complex in airspace network and requires fine and flexible management, it is difficult to guarantee the system efficiency and safety level.

The flight sorting and dispatching method of the regional multi-airport terminal area in the traditional civil aviation field is used as the baseline. This paper designs a complete MVS-TA adaptive management system including route structure, control rules and scheduling optimization, which aims to improve the operation efficiency of MVS-TA in medium–high density areas at an acceptable safety level. The contributions of this paper include three aspects: 1) In view of the characteristics of the dense distribution of vertiports, the concept of MVS and the structure design of multi-ring are put forward. 2) By adding the road capacity constraints into the backpressure strategy, a model of the intersection control rules of MVS-TA is constructed 3) The integrated adaptive scheduling model, which includes the dynamic time-saving path planning model and the sequencing model at the transit junction, is proposed to realize the coordinated scheduling of approach-departure flights and distributed control.

The rest of this paper is organized as follows: Section II designed the multi-ring operation structure for the MVS terminal area, and constructed the control rules of junctions based on the cyclic phase backpressure strategy. Based on traffic structure and operation control rules, Section III constructs the integrated adaptive scheduling model for MVS. Section IV combs the implementation framework and algorithm flow of the ACS. Example simulation and result analysis are described in section V. Section Vl concludes the paper.

2. The conceptual structure and operating rules of the multi-vertiport system

According to the operation characteristics and the flight process of eVTOL, this section designs a route structure including multiple rings and transit junctions for the Terminal Area of Multi-vertiport system (MVS-TA), which is the main innovation of this chapter. Further, the backpressure control strategy is introduced into UAM's intersection control and segment capacity constraints are added to make it more applicable.

A vertiport has one or more vertical take-off and landing platforms (vertipads). The conceptual structure and operation rules of MVS-TA described in this section focus on the terminal area and do not involve the scheduling rules between the vertipads of each vertiport. Moreover, the conceptual structure and operating rules described in this section are also applicable to the terminal area of a single vertiport with multiple vertipads. Without considering the optimal scheduling between vertipads, the integrated adaptive scheduling model (section 3) is also applicable.

2.1. The conceptual structure and system modeling of MVS-TA

2.1.1. The conceptual structure of MVS-TA

The current growth in commercial air traffic has outpaced the capabilities of people-centered systems, and this is only for manned flights. The growth of unmanned and autonomous aircraft will increase traffic by several orders of magnitude. NASA predicts that as UAM reaches maturity (UML-5), a city will accommodate more than 1,000 eVTOL aircraft in a typical 30 to 40n mile diameter range, with airspace density 400 times the allowable IFR density (Mueller, 2019). Constraints on air traffic control workload are a key factor limiting the speed and density of UAM operations. Developing concepts, techniques, and procedures for UAM to manage without air traffic control tactical intervention, and implementing rule-based information communication of system elements, is an important part of achieving higher density, faster-paced UAM operation (Thipphavong et al., 2018). Therefore, this paper starts from the route structure and operating rules of MVS-TA to ensure the safe and efficient operation of medium–high density approach-departure flights in complex airspace.

The operation schedule of the flights is based on a new generation of CNS (communication, navigation, and surveillance) networks (e.g. VHF OMF VOR, WIDE Enhancement System, etc.) and high-capacity, low-latency precision guidance for navigation equipment (Thipphavong et al., 2018*)*. Each eVTOL is the subject of the CNS network. Ground base stations can collect real-time data and transmit information to each aircraft during operation. Each aircraft can also clarify the location information of other flight subjects (including traditional flights) within a certain range while receiving the ground base station dispatch instructions. The system's CNS network and data transmission are particularly important in areas with low visibility, large buildings, and densely populated areas.

Specifically, the MVS-TA designed in this paper is a radiant structure (Fig. 1) including the approach-departure rings, emergency ring, junctions, approach-departure routes, and waiting areas (holding stack). The ring layers are concentric circles with different radius and heights, which form the "frustum of a cone" shape (Fig. 2), to accommodate the operating characteristics of frequent altitude changes as the aircraft enters/leaves the terminal area. The vertical take-off and landing point is 200 m away from the vertiport, which is the transition point between the vertical flight and the approach-departure program. The system consists of several vertiports$V = \{V_1, V_2, \cdots, V_N\}$ and approach-departure rings. The outermost ring layer (Starting ring layer$Ring_A$) is the boundary between the terminal area and other airspaces. The middle ring layer and the final ring layer are used for route planning and scheduling of flights. They are divided into two parts by the line passing through the diameter of the concentric circle: the approach ring layer

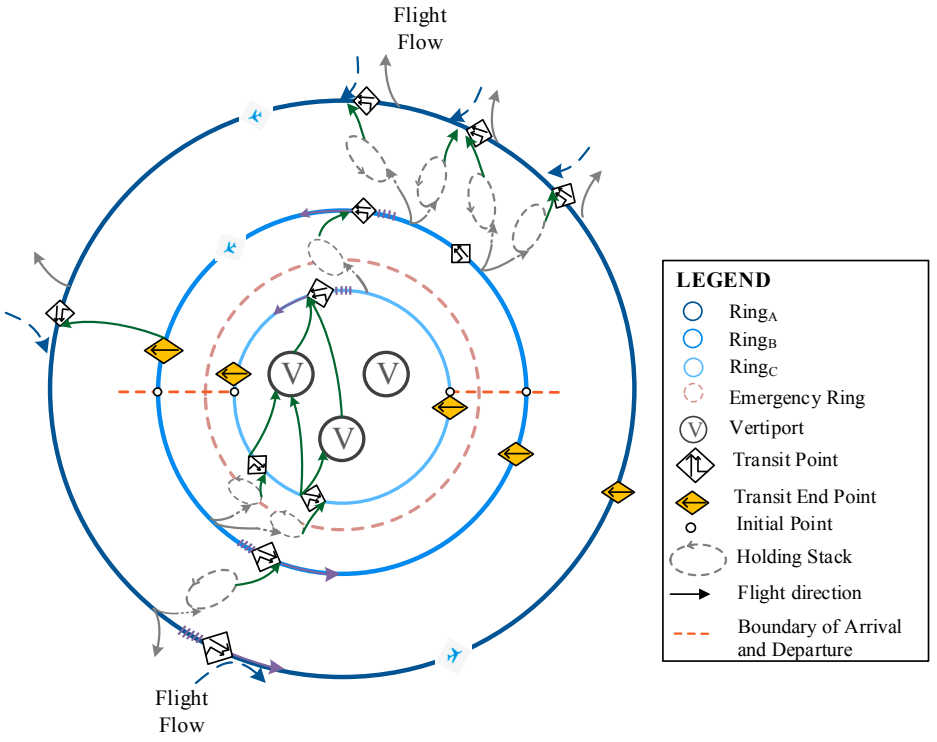

Fig. 1. Operational concept design for terminal airspace of MVS-TA.

(Middle approach layer $Ring_{A-B}$, Final approach layer $Ring_{A-C}$) and departure ring layer (Middle departure layer $Ring_{D-B}$, Final departure layer $Ring_{D-C}$). The approach side and the departure side switch in different directions but connected, the aircraft can operate around the ring layer. Each ring level includes several transit junctions.

Relatively speaking, each transit junction is an important node for frequent changes of aircraft altitude and speed and is an area with a higher risk of dangerous approach. The location planning should not only take into account the airspace structure and the ground base station, but also control and reduce the impact of the operation on the ground buildings and personnel from a safety perspective. This aspect is not within the scope of this article.

Transit junctions can control and dispatch the flow based on the traffic signal issued by the ground base station. According to the difference of control mode, the junctions can be divided into three categories: initial transit junction, composite junction, and transit endpoint. 1) The initial transit junction is the initial node of the switching ring layer (Fig. 4e). 2) The composite intersection structure includes shadow nodes and signal-controlled points. In order to reduce the control load and the risk conflict at the junction, the flight

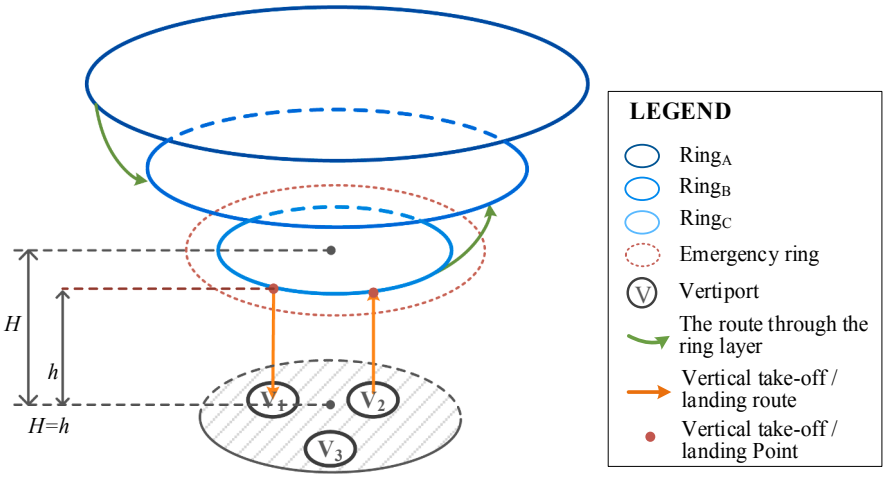

Fig. 2. Three-dimensional diagram of operational concept for MVS-TA.

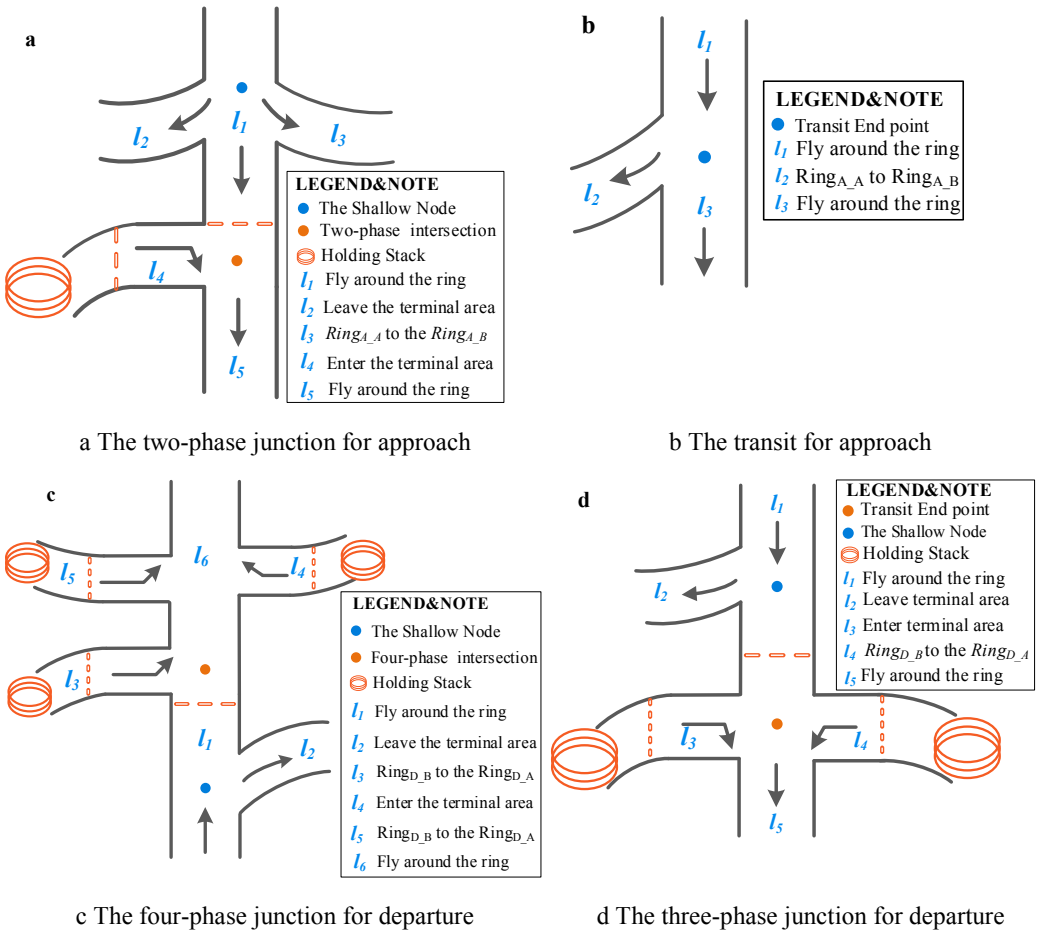

Fig. 3. The intersection structure of.$Ring_A$

flow can only sink out of the ring layer at the "shadow node" in front of the multi-phase transit junction, which is not controlled by the signal light. Flights are only allowed to around or sink into the ring layer in accordance with signal control at each multi-phase transit junction (Fig. 3). 3) The shadow node before the transit endpoint is the last chance for the flight flow in the ring to switch to the inner ring layer. Due to the functional differences of each ring layer in the system, the characteristics of the transit junctions between the different height ring layers and between the approach-departure ring layers are slightly different. $Ring_A$ contains only multi-phase transit junctions and control endpoints (Fig. 3), where approach-departure flights make flight orientation adjustments. $Ring_B$ and $Ring_C$ contain three types of transit junctions (Fig. 4), which realize the adaptive scheduling and improve the operational efficiency through signal control and sequencing optimization of each junction.

The characteristics of MVS-TA system are summarized as follows: 1) The structure consists of three approach-departure ring layers and one emergency ring layer, which are applied to normal operation and emergency respectively. Flights in emergency situations can operate on the emergency ring, greatly reducing the impact on normal operations of other flights. 2) The operation control of the intersection can greatly reduce the flight conflict from the mechanism. 3) The radiant structure can improve the capacity, operational efficiency, and utilization of airspace resources in the terminal area. The "frustum of a cone" shape is more suitable for the eVTOL operation. 4) Due to the competition in time and space resources (such as air routes and intersections, etc.), there is competition between vertiports.

2.1.2. A modeled description of the transit junctions of MVS-TA

The traffic network in the MVS-TA can be modeled as a forward figure G containing M transit junctions. The set of transit junctions includes several junctions, which can be expressed as$J = \{j_1, j_2, \cdots j_M\}$. Each junction j_i includes three partsL_i、F_i、P_i, representing the set of links, the set of aircraft traffic flows, the set of phases. The link collection$L_i = \{l_i^1, l_i^2, \cdots, l_i^N\}$, can be divided into two subsets: the set of input links $L_{in}(j_i)$ and the set of output links $L_{out}(j_i)$.

Suppose the two-phase intersection represented by Fig. 3a is defined as j_1. l_1^1 and l_1^4 are both input links, and l_1^5 is the output link, i.e.

$$L_{in}(j_1) = \{l_1^1, l_1^4\} \tag{1}$$

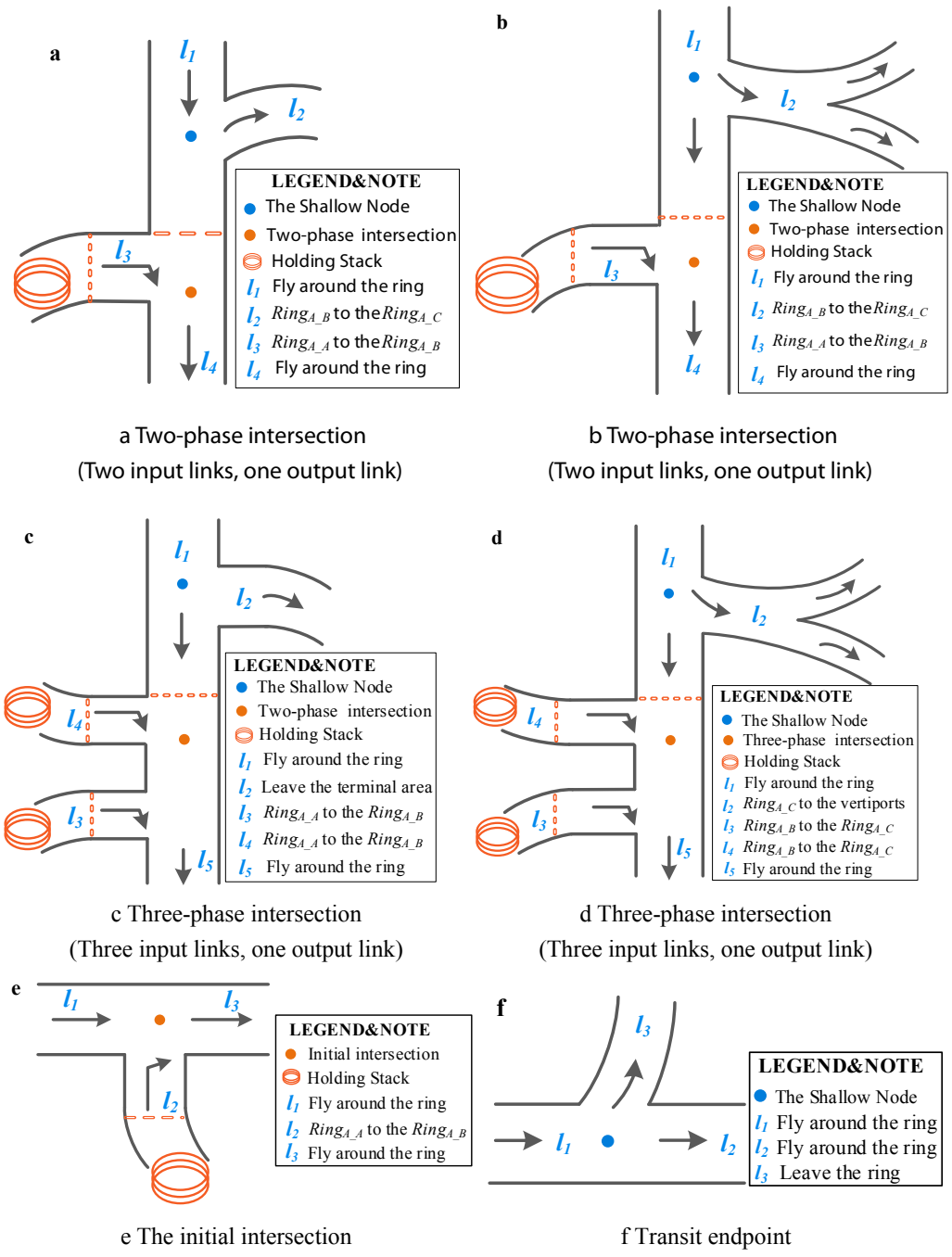

Fig. 4. The intersection structure of the approach side ring layer $Ring_{A-B}(Ring_{A-C})$ (Note: The junctions of $Ring_{D-B}$ and $Ring_{D-C}$ on the departure side are similar to the approach side. Fig. 4a-Fig. 4d are composite junctions with different multi-phase junction).

$$L_{out}(j_1) = \{l_1^5\} \tag{2}$$

The process of aircraft passing through each junction can be regarded as a traffic movement process. When two adjacent links have a feasible path, traffic flows can be transferred from the upstream link to the downstream link. The transfer rate is equal to the saturated rate when the upstream link is oversaturated and is considered 0 when there are no channels between the two adjacent links. Therefore, when the upstream is oversaturated, the number of aircraft transferred through the corresponding channel is a product of the green light time and saturation flow rate (flight interval is considered). For the flight process collection FD_i of the junction j_i, there is $fd_i^{ab} \in FD_i$, where fd_i^{ab} is the traffic flow from the input link l_i^a to the output link l_i^b, $l_i^a \in L_{in}(j_i), l_i^b \in L_{out}(j_i)$. There is a variety of traffic

flow transfer processes at each junction,$L_{in}(j_i) \times L_{out}(j_i)$, which are controlled by different phases to give them access.p_i^k represents the kth phase of the transit junctionj_i, $P_i$is a collection of all phases of junction j_i.

$$FD_i = L_{in}(j_i) \times L_{out}(j_i) = \{fd_i^{ab}\} \tag{3}$$

$$P_i = \{p_i^1, \cdots, p_i^k, \cdots p_i^K\} \tag{4}$$

2.2. Cyclic phase backpressure control traffic signal control at junctions

To realize the adaptive control at junctions of MVS-TA, this paper describes the queuing process of junctions based on the dynamic queuing model, and calculates the allowable pass time for each phase by using the Cycle Phase Backpressure (CPB) policy adapted to the flight operation.

In the control model, the time parameters are modeled as discrete, i.e., based on a slotted time model. $tp = 1, 2, \cdots$ represents the number of the period about to be initiated. Assuming that the cycle length of each transit junction isTP, each link has only one flight path. Control decisions in CPB policy are made at the beginning of each time cycle (so it is a fixed cycle policy which is similar to the policy in (Le et al., 2015)). At the beginning of each control cycle, the ground navigation device can update the data in the next cycle, including the queue data and the green time assigned to each phase p_i^k. Compared with ground traffic, due to the need to control the interval of flights passing through intersections, the buffer time of traffic lights is not set, that is, the total period length is equal to the effective period length.

2.2.1. Queue dynamics model

References to relevant literature (Hao, 2019; Le et al., 2015; Ma et al., 2020), this section provides a quantitative description of the dynamic queuing model on the air route. For junctionj_i, at the beginning of the tp window, the number of aircraft queuing on link l_i^a and entering link l_i^b is $Q_{ab}(tp)$, and the total number of aircraft queued on link l_i^a is $Q_a(tp)$, which means:

$$Q_a(tp) = \sum_{l_i^b \in L_{out}(j_i)} Q_{ab}(tp) \tag{5}$$

At the beginning of the $tp+1$ window, the number of aircraft queued on link l_i^a and entered linkl_i^b,$Q_{ab}(tp+1)$, can be expressed as:

$$\begin{aligned} Q_{ab}(tp+1) = Q_{ab}(tp) &- \{\text{The number of flights flying from } l_i^a \text{ to } l_i^b \text{ during } tp \text{ period.}\} \\ &+ \{\text{The ratio of the flight flying from } l_i^a \text{ to } l_i^b.\} * \{\text{During } tp \text{ period, the upstream links increase the number of flights on } l_i^a\} \end{aligned}$$

$\varphi_{p_i^k}(tp)$ is the proportion of green light time of the phase p_i^k controlling traffic fd_i^{ab}, and this value calculation will be detailed in section 2.2.2. If link l_i^a is saturated during tpperiod, the number of aircraft from l_i^a to l_i^b is the product of the rate $SR_{ab}(tp)$ and the corresponding phase time allowed, otherwise the value is $Q_{ab}(tp)$. Therefore, $Q_{ab}(tp+1)$ can be quantified as:

$$Q_{ab}(tp+1) = Q_{ab}(tp) - \left\{ \left[SR_{ab}(tp) \bullet \varphi_{p_i^k}(\mathrm{tp}) \bullet \mathrm{TP} \right] \wedge \mathrm{Q_{ab}(tp)} \right\} + \mathrm{R_{ab}(tp)} \sum_{c \in \Gamma_a^+} \left\{ \left[\mathrm{SR_{ca}(tp)} \bullet \varphi_{p_i^k}(\mathrm{tp}) \bullet \mathrm{TP} \right] \wedge \mathrm{Q_{ca}(tp)} \right\} \tag{6}$$

Where, define $x \wedge y = \min(x, y)$. For $fd_i^{ab} \in FD_i$, $R_{ab}(tp)$ is the turning rate, i.e. the ratio of the number of vehicles entering l_i^b from l_i^a during cycle tp to the total number of vehicles on l_i^a, which satisfies $\sum_{l_i^b \in L_{out}(j_i)} R_{ab}(tp) = 1$.

The turning ratio for vehicles entering link l_i^a within cycle tp cannot be calculated at the beginning of the cycle (Ma et al., 2020). Assuming that the upstream link of the intersection is equally likely to enter each downstream link, the initial value of this parameter is estimated. Based on the homogeneity of aircraft (Le et al., 2015), the value of $R_{ab}(tp)$ is updated in the process of simulation. The homogeneity of aircraft means each car at the junction has the same likelihood of joining each subsequent junction. When the system collects a large amount of flight operation data in practice, it is available to determine the stable value of $R_{ab}(tp)$ at different times of the day.

$$R_{ab}(tp) = \frac{1}{N} \sum_{tp=1}^{tp} \frac{QL_{ab}(tp)}{QL_a(tp)} \tag{7}$$

tp is the current cycle number. $QL_{ab}(tp)$ and $QL_a(tp)$ are the number of flights in the tp period that are sent by linkl_i^a to the linkl_i^b and the total number of flights on the l_i^a link, respectively. N is the number of periods used to calculate the probability of turning.

2.2.2. Cyclic phase backpressure control policy—traffic control rules at junctions

Backpressure control policies were originally developed by (Tassiulas and Ephremides, 1992) for routing and scheduling of packet transmission in a wireless network. Later, backpressure strategies were used to control traffic signals for urban ground traffic(Varaiya, 2013a, 2013b; Wongpiromsarn et al., 2012). This section uses the backpressure policy with fixed cycle time and cyclic phases to control the traffic flow at the intersection, which is an improved control method of the original strategy. The main advantage of the CPB control policy is: 1) Unlike centralized optimization structures with high traffic and computation, this strategy is a distributed optimization control method that requires traffic flow control based on information about the appropriate control points and adjacent links. 2) This strategy can obtain traffic network feedback in real-time and dynamically adjust the signal control scheme at the beginning of each cycle to optimize intersection throughput (Le et al., 2015).

Similar to ground transportation, a signal control that manages traffic flow in different directions is defined as a phase. The system control is based on the communication navigation monitoring network. The total time required to complete a set of signal indications in each traffic flow direction is called the cycle length of the intersection. The transit junction is an important node to control the traffic flow and reduce the collision risk from the mechanism. According to the traffic volume of different phases, CPB strategy can allocate more allowed passing time for the phases with large traffic flow in each period, and realize the maximum throughput and stable control of the traffic network.

Because the CNS network can monitor the number of aircraft queuing at each intersection in real-time, the CPB policy controls traffic based on the queue length. For the same intersection, the larger the backpressure weight of the phase, the longer the passing time assigned. According to the queue length, turn probability and saturation flow rate, the backpressure weight and the proportion of green time of the next period are calculated at the beginning of each cycle.

The calculation process of CPB policy is as follows:

During the tp period, the pressure weight generated by traffic flow fd_i^{ab} is the queue length $Q_{ab}(tp)$ at l_i^a minus the average queue length at the output linkl_i^b, which can be expressed as

$$pressure_{ab}(tp) = Q_{ab}(tp) - \sum_{c \in out_b} R_{ab}(tp) \bullet \mathrm{Q_{bc}(tp)} \tag{8}$$

During the tp period, the pressure weight of p_i^k (the kth phase of the transit junctionj_i) is accumulated by the pressure weight of traffic flows controlled by that phase (Eq. (9)).

$$W_{p_i^k}(tp) = \sum_{fd_i^{ab} \in p_i^k} pressure_{ab}(tp) \bullet \mathrm{SR_{ab}(tp)} \tag{9}$$

According to the backpressure weight of each phase at the beginning of the current period of the intersection, the division ratio of the green time of each phase can be calculated. The proportion of green light time of each phase p_i^k can be expressed as Eq. (10).

$$\varphi_{p_i^k}(tp) = \frac{\exp[\eta \bullet W_{p_i^k}(tp)]}{\sum_{p_i^* \in P_i} \exp[\eta \bullet W_{p_i^*}(tp)]} \tag{10}$$

Each weight value can be positive or negative, and the green light time ratio is always positive. You can adjust η by adjusting the parameters and parameters. The green light time ratio for each phase of junction j_i is satisfied Eq. (11).

$$\sum_{p_i^k \in P_i} \varphi_{p_i^k}(tp) = 1 \tag{11}$$

Assuming that the aircraft on each link comes from its upstream link, the remaining capacity of link l_i^a at the beginning of the period $tp+1$ is directly related to the flight flow of the upstream link $f_a^{in}(tp)$ and the downstream link $f_a^{out}(tp)$ in tp period, where $f_a^{in}(tp)$ and $f_a^{out}(tp)$ are calculated similarly to Eq. (6).

$$\begin{aligned} QL_a(tp+1) &= min\{QL_a(tp) + f_a^{in}(tp) - f_a^{out}(tp), C_a^{max}\} \\ C_a^{rem}(tp+1) &= C_a^{max} - QL_a(tp+1) \end{aligned} \tag{12}$$

$$\begin{aligned} f_a^{in}(tp) &= \sum_{c \in \Gamma_a^+} \{[SR_{ca}(tp) \cdot GT_{ac}(tp)] \wedge [QL_c(tp) \cdot R_{ca}(tp)]\} \\ GT_{ac}(tp) &= \varphi_{p_i^k}(tp) \cdot TP, fd_i^{ac} \in p_i^k \end{aligned} \tag{13}$$

$$f_a^{out}(tp) = \sum_{b \in \Gamma_a^-} \{[SR_{ab}(tp) \bullet \mathrm{GT_{ab}(tp)}] \wedge [\mathrm{QL_a(tp)} * \mathrm{R_{ab}(tp)}]\} \tag{14}$$

Where C_a^{max} represents the maximum capacity (capacity threshold) of the link, $C_a^{rem}(tp)$ represents the remaining capacity of link l_i^a at the beginning of cycle tp. Γ_a^+ and Γ_a^- represent the upstream-link collection of link l_i^a and the downstream-link collection of link l_i^a, respectively. $QL_a(tp)$ is the total traffic of segment l_i^a of the tp period. Flights from l_i^a to l_i^b are controlled by the appropriate phase at the intersection. $GT_{ab}(tp)$ represents the allowed pass time (green light time) for that phase during the tp period.

It is important to note that the usual fixed phase sequence control method has a minimum green light pass time limit for each phase,

i.e. the phase where the link is about to overflow (the backpressure weight is very small) is also assigned a minimum green time (Ma et al., 2020), which is not allowed in the safety-demanding terminal area scheduling. Because the location of the aircraft and the load of each link can be monitored with the CNS network, the remaining capacity of the air traffic link can be quantified more accurately. This paper takes into account the capacity limitations of each link: 1) the minimum green light pass time is not considered in the allocation of green time for each phase; 2)The number of flights passing through each phase should be satisfied Eq.15, and overloaded flights need to wait at intersections or choose other routes. The junctions shall control that the load of each link is less than its maximum capacity ($QL_a(tp) \le C_a^{max}$), and the load of the corresponding ring layer is also less than its capacity threshold.

$$\sum_{fd_i^{ab} \in p_i^k} QG_{ab}(tp) \le C_b^{max} - QL_b(tp) \tag{15}$$

Where $QG_{ab}(tp)$ is the number of flights allowed through the phase p_i^k in tp cycle.

3. The integrated adaptive scheduling model for approach-departure flights

3.1. Problem description

The integrated adaptive scheduling model to solve the problem is: Based on the operating characteristics of eVTOL and the designed operating environment, how to schedule and optimize the operation of flights in the terminal area to minimize the cost of flight delay.

In this section, the adaptive control model of MVS-TA is proposed, including two sub-models, which are the shortest path planning model based on the dynamic traffic network and the distributed sequencing at junctions. Given the destination vertiport and the boundary point from the terminal area, each aircraft can dynamically adjust the flight path and pass through the intersections in sequence and at intervals. It is worth noting that the traditional flight scheduling method is usually to sort and optimize all flights throughout the optimization period, and the calculation pressure is relatively large in the case of large flight volume. The adaptive control model in this article is calculated for queued flights at each intersection. The implementation of distributed optimization can greatly reduce the control pressure of the central controller.

The model built in this article is based on the following premises:

(1) In this paper, it is considered that flight collisions can be avoided, and safety can be ensured through safe separation and intersection rules, as well as the CNS network. The risk assessment of the terminal area is not within the scope of this paper.
(2) The model constructed is aimed at flight scheduling in the MVS-TA, without considering the number of vertipads in the vertiport. Under the premise of not considering the scheduling between vertipads, the model can also be applied to the terminal-area scheduling of a single vertiport with multiple vertipads.
(3) The terminal area scheduling structure of this paper is set to medium flight density, and the capacity limit of Holding Stack is not considered.

Based on the traffic network structure and control rules of the transit junction of the MVS-TA, combined with the operating characteristics of eVTOL, this section constructs the integrated adaptive scheduling model as follows:

3.2. The shortest path planning model based on the dynamic traffic network

eVTOL as a vehicle and mobile load carrier, its travel distribution and route selection will affect the operation efficiency of the terminal area route, while the remaining electricity, range, etc. will affect the safety level of the system. On the other hand, the topology and control rules of the traffic network in the terminal area will affect the path planning of eVTOL from the ground base station. Therefore, “eVTOL state- path planning - control rules ” are related and affected by each other. Based on MVS-TA structure and intersection control rules, this section puts forward the update mechanism of dynamic traffic network, depicts the effect of terminal segment traffic on eVTOL running time, and constructs the shortest route planning model based on dynamic traffic network.

3.2.1. Dynamic traffic network modeling

(1) Route impedance model

First, the road resistance function is constructed to describe the cost of the flight during the approach and departure. Based on the commonality of air traffic and ground traffic, as well as the correlation between traffic flow speed-flow-density, the basic relationship between traffic flow and travel time can be obtained. (Hao, 2017; Sun, 2020; Wang et al., 2006; Xu et al., 2015):

$$t = t_0 \left(\frac{2}{1 + \sqrt{1 - \frac{q}{C}}} \right) \tag{16}$$

Traffic flow represents the number of traffic entities passing through a segment or section during a period, the value of which is

constantly changing with time and space, and the traffic flow at a certain time is not of sufficient practical significance. This paper selects the traffic network real-time update mechanism with tp as the update cycle(Cui, 2013), so the average $\overline{QL_a}$ and saturation $S_a(tp)$ (Eq. (17)) are calculated by the flow of the adjacent period of l_i^a. The road resistance of segment l_i^a updated in the cycle tp can be further available (Eq. (18)).

$$S_a(tp) = \frac{\overline{QL_a}}{C_a^{max}} = \frac{[QL_a(tp) + QL_a(tp+1)]}{C_a^{max} \bullet 2}, (tp-1)TP \le st_j^f \le tp \bullet \mathrm{TP} \tag{17}$$

$$W_{ij}(tp) = t_0\left(\frac{2}{1-\sqrt{1-S_a(tp)}}\right) \tag{18}$$

$S_a(tp)$ indicates the saturation of segment l_i^a in the period to which time st_j^f belongs, which is the ratio of the average traffic volume to the capacity of the corresponding route, and $S_a(tp) \le 1$. st_j^f indicates the time at which the aircraft $f$reaches the transit junction j_i. If condition $(tp-1)TP \le st_j^f \le tp \bullet \mathrm{TP}$ is met, st_j^f belongs to the tp cycle.

(2) The traffic network topology of MVS-TA

Taking the road resistance as the weight, the route network of MVS-TA is constructed by a topological relationship, with nodes (such as v_k,v_q) representing intersections and arcs representing the connections of each road.

The route network is defined as $\boldsymbol{G^T} = (\boldsymbol{V}, \boldsymbol{E}, \boldsymbol{A}, \boldsymbol{C})$, where $\boldsymbol{V}$ is the set of nodes, $\boldsymbol{A}$ is the road weight set, $\boldsymbol{C}$ is the capacity of the road, $\boldsymbol{E}$ is the collection of all the curved segments, that is, the collection of all segments in the terminal area.

$$a_{kq} = \begin{cases} w_{kq}(tp), \ v_{kq} \in E, \ \text{the resistance of } v_{kq} \\ 0, \ v_k = v_q \\ \infty, \ v_{kq} \notin E \text{ or Reach the threshold of } v_{kq} \end{cases} \tag{19}$$

$\boldsymbol{A} = (a_{kq})_{K \times K}$ describes the road lengths, the connections of the nodes, the one-way or two-way access, and the road resistance characteristics. The segment of the terminal area in this paper is one-way access. Its element value $w_{kq}(tp)$ is updated with the number of flights on the corresponding road. Adjacent matrix $\boldsymbol{A}$ can be generally expressed as Eq. (20) (Luo et al., 2016).

$$\boldsymbol{A} = \begin{bmatrix} 0 & w_{12}(tp) & w_{13}(tp) & \cdots & w_{1K}(tp) \\ w_{21}(tp) & 0 & w_{23}(tp) & \cdots & w_{2K}(tp) \\ w_{31}(tp) & w_{32}(tp) & 0 & \cdots & w_{3K}(tp) \\ \vdots & \vdots & \vdots & \ddots & \vdots \\ w_{K1}(tp) & w_{K2}(tp) & w_{K3}(tp) & \cdots & 0 \end{bmatrix} \tag{20}$$

Therefore, $\boldsymbol{G^T}$ can be expressed as Eq. (21).

$$\begin{cases} \boldsymbol{G^T} = (\boldsymbol{V}, \boldsymbol{E}, \boldsymbol{A}, \boldsymbol{C}) \\ \boldsymbol{V} = \{v_k | k = 1, 2, \cdots, K\} \\ \boldsymbol{E} = \{v_{kq} | v_k \in \boldsymbol{V}, v_q \in \boldsymbol{V}, k \ne q\} \\ \boldsymbol{A} = \{w_{kq}(tp) | v_{kq} \in \boldsymbol{E}, (tp-1)TP \le st_j^f \le tp \bullet TP\} \\ \boldsymbol{C} = \{C_a^{max} | a \in L\} \end{cases} \tag{21}$$

3.2.2. The shortest path planning model

Based on the section 3.2.1, the road resistance of each section varies dynamically with the change of saturation, which can realize the real-time update of the traffic network. When the aircraft reaches each transit junction, the system plans and guides its path from the current position $L_s(f)$ to the destination $L_d(f)$. The time at which the aircraft reaches its current position is st_j^f. The time for the aircraft to arrive at the destination $t_d(f)$ is the accumulation of the road resistance of the actual driving path $R_p(f)$:

Table 1
three-dimensional priority of flights.

	State of Charge R = 1		State of Charge R = 2		State of Charge R = 3	
	Approach O = 1	Departure O = 2	Approach O = 1	Departure O = 2	Approach O = 1	Departure O = 2
mission characteristics V = 1	1	2	4	8	10	18
mission characteristics V = 2	3	6	9	16	19	31

$$t_d(f) = st_j^f + \sum_{v_{ij} \in R_p(f)} \left(v_{kq} \bullet \mathrm{w_{kq}(tp)}\right) \tag{22}$$

$$v_{kq} = \begin{cases} 1, v_{kq} \in R_p(f) \\ 0, v_{kq} \notin R_p(f) \end{cases} \tag{23}$$

In the current route network state, seek the shortest time path planning for each flight from the current point to its destination to determine the next node and the next route to be flying, which can be expressed as Eq. (24).

$$\min W_f = \min t_d(f) = \min \left(st_j^f + \sum_{v_{kq} \in R_p(f)} \left(v_{kq} \bullet \mathrm{w_{kq}(tp)}\right) \right) \tag{24}$$

3.3. Distributed scheduling model for flights at junctions

3.3.1. Objective function

The position adjustment involved in the sorting work will bring some control load and risk to the aircraft, so the aircraft sorting work is completed within the waiting time of the intersection. Transit junction is the key node in the flight path, not only to update the shortest-time path according to traffic network obstruction, but also to sort the queue for flights according to the importance. Considering the safety, the goal of the model proposed in this paper is to minimize the total comprehensive running time through each transit intersection under the constraints of the safe interval, take-off and landing interval, and battery charge state.

The number of flights waiting to pass through junction j is n_F^j. Flight f arrives at the terminal area at ETA_f and is allowed to pass junction j at et_f^j. The combined operating time of each flight at each junction can be expressed as Eq. (25).

$$Delay_f^j = Imp_f\left(st_f^j\right) \bullet \left|\mathrm{et_f^j} - \mathrm{ETA_f}\right|, \mathrm{f} = 1, 2, \cdots, \mathrm{n_F^j}; \forall \mathrm{j} \in \mathrm{J} \tag{25}$$

$$Imp_f(t) = \lceil M / prior_f(t) \rceil \tag{26}$$

$Imp_f(t)$ is the important factor of flight f at the moment t, which is related to the flight's approach-departure attribute, mission characteristics and the State Of Charge (SOC), and is reflected by the priority $prior_f(t)$ of the flight. M is the largest number in the priority table (Table 1). In this section, the time parameter t is measured as a moment node in the timeline (intervals of 1 s), $\mathrm{t} \in \mathrm{T}$.

The optimization goal of sequencing is to minimize the combined running time of queued flights at the junction:

$$\min \sum_{f=1}^{n_F^j} Delay_f^j = \min \sum_{f=1}^{n_F^j} Imp_f(st_f^j) \bullet \left|\mathrm{et_f^j} - \mathrm{ETA_f}\right|, \mathrm{f} = 1, 2, \cdots, \mathrm{n_F^j}, \forall \mathrm{j} \in \mathrm{J} \tag{27}$$

3.3.2. Constraints

Since the green pass time for each phase, i.e., the pass window, is limited, the ordering of the current phase can end when the optimized departure time et_f^j of the last flight in the sorted flight exceeds the pass window boundary of the next signal cycle. The remaining unsorted flights need to wait for the next cycle red light and sort.

Assuming that eVTOL flight power consumption increases linearly over travel time, ground base stations can obtain the SOC of aircraft f in real time. The aircraft's SOC is $SOC_f(st_f^j)$ when arriving at junction j. This parameter tracks the status of the vehicle's power from full (1.0, 100%) to empty (0.0), which can be expressed as Eq. (28).

$$SOC_f(st_f^j) = \gamma\left(SOC_f^0 - E_c \bullet \left(\mathrm{ETA_f} - \mathrm{st_f^j}\right)\right) \tag{28}$$

γ is the energy consumption factor, the value range is [0.9,1]. SOC_f^0 is the SOC of flight f when entering the terminal area. E_c is the power consumption per unit time (s) of the aircraft.

The constraints on the scheduling model of queued flights at each intersection are as follows:

Sets

F	The set of flights to be optimized.
J	The set of junctions in the terminal area system.
U	The set of the vertiports.

Parameters

st_f^j	The time when flight f arrives at the intersection j.
ETA_f	The time when flight f arrives at the terminal area (refers to the arrival of the approach-flight to the outer ring boundary or departure flight ready to take off).
$ST_{u,f}$	The landing/take-off time of flight f at vertiport$u$
$\sigma_{ff'}$	The minimum take-off and landing interval.
$\delta_{ff'}$	The minimum safe separation of the junctions.
P_{sf}^j	The initial queuing position of flight f at junction j.
$SOC_f(t)$	The State Of Charge on flight f at t.
$GS_{p_j^k}(f,tp)$	Assuming that flight f reaches the intersection$j$ during the tp period, and the direction of the next route is controlled by phase p_j^k, $GS_{p_j^k}(f,tp)$ is the green light start time of the phase p_j^k.
$G_{p_j^k}(f,tp)$	The green light duration of the phase p_j^k.
$Q_{ab}\left(st_f^j\right)$	The number of queues at the intersection at st_f^j.
P^R	The limit of the position adjustment range.

$$ES_f(t) = \begin{cases} 0, & \text{if } SOC(t) \le 16\% \text{ or Flight } f \text{ is in an emergency} \\ 1, & \text{otherwise} \end{cases}$$

$$EP_{fj} = \begin{cases} 1, & \text{if } st_f^j < GS_{p_j^k}(f,tp) \text{ or } st_f^j \ge G_{p_j^k}(f,tp) + GS_{p_j^k}(f,tp), \text{or } Q_{ab}\left(st_f^j\right) \ne 0 \\ 0, & \text{otherwise} \end{cases}$$

$$\forall j \in J, (tp-1)TP \le st_j^f \le tp \cdot TP$$

$$\rho_{ff'} = \begin{cases} 1, & \text{if flight } f' \text{ is in the adjacent previous position of flight } f \\ 0, & \text{otherwise} \end{cases}$$

$$w_{ff'} = \begin{cases} 1, & \text{if flight } f \text{ and } f' \text{ are at the same intersection} \\ 0, & \text{otherwise} \end{cases}$$

$$\lambda_{ff'} = \begin{cases} 1, & \text{if flight } f \text{ shares the same vertiport with } f' \\ 0, & \text{otherwise} \end{cases}$$

$$EQ_{fj} = \begin{cases} 1, & \text{if flight } f \text{ is required to queue at intersection } j \\ 0, & \text{otherwise} \end{cases}$$

$$ord = \begin{cases} 1, & \text{Flight } f \text{ is the first in the queue}(P_{sf}^j = 1) \\ 0, & \text{otherwise} \end{cases}$$

Decision variables

et_f^j	The time when the flight f leaves the intersection$j$
P_{ef}^j	The final optimization position of the flight f at the junction.

Constraints

$$ES_f\left(st_f^j\right) + EP_{fj} - 1 \le EQ_{fj} \tag{29a}$$

$$\left[ES_f\left(st_f^j\right) + EP_{fj}\right] \Big/ 2 \ge EQ_{fj} \tag{29b}$$

$$et_{f'}^j + \delta_{ff'} - M'(1 - w_{f,f'}\rho_{f,f'}) \le et_f^j, \forall f, f' \in \mathrm{F}; \forall \mathrm{j} \in \mathrm{J} \tag{29c}$$

$$ST_{u,f'} + \sigma_{ff'} - M'(1 - \lambda_{f,f'}\rho_{f,f'}) \le ST_{u,f}, \forall f, f' \in \mathrm{F}; \forall \mathrm{u} \in \mathrm{U} \tag{29d}$$

$$et_f^j - GS_{p_j^k}(f) \ge M'(ord - 1), \forall f \in \mathrm{F}; \forall \mathrm{j} \in \mathrm{J} \tag{29e}$$

$$P_{ef}^j - P_{sf}^j \le P^R, \forall f \in F; \forall j \in \mathrm{J} \tag{29f}$$

$$P_{sf}^j - P_{ef}^j \le P^R, \forall f \in F; \forall j \in \mathrm{J} \tag{29g}$$

$$\begin{cases} if\ EQ_{fj} = 0, et_f^j = st_f^j \\ if\ EQ_{fj} = 1, P_{sf}^j \ge 1, P_{ef}^j \ge 1 \end{cases} \tag{29h}$$

Eq. (29a) – (29b) determines whether flight f is queued according to the SOC and the arrival time at the junction, which are constraints related to the queue status of intersection j. If the SOC of flight f is less than 16%, or the flight has other unexpected conditions, ES_f is 0. The flight is dispatched to the emergency ring floor and can be reached directly to the planned airport without

having to wait in line. For flights with SOC greater than 10%, if the phase at the junction is green and there are no queued flights at st_f^j, $EP_{fj} = 0$, it can pass at the specified interval. Otherwise, the flight will need to be suspended waiting in line and the service system will sort the waiting list. When $ES_f\left(st_f^j\right) = 1 and EP_{fj} = 1$, flight f waits at junction j (Eq.29a).

Eq. (29c) ensure that the adjacent waiting flight f and $f^{'}$ at junction j meet the separation requirements (Separation Norms). Eq. (29d) is the interval constraint of vertiport $u.M$' is an infinite positive number. Eq. (29e) ensures that the first flight in the order leaves the intersection at the time after the green light $GS_{p_j^k}(f)$ of the next period in the corresponding phase p_j^k. Considering the safety and ensuring that flights are not delayed too long due to sequencing, the queuing position adjustment constraint of flight f at junction j is described by Eq. (29f) and Eq. (29g). Eq. (29h) describes the relationship between EQ_{fj}, et_f^j and P_{sf}^j.

When optimizing flight order at intersections, the differences in priority levels due to the flight's specific attributes must be considered. This paper calculates the main factors of priority from the SOC, mission characteristics and the mode of operation (take-off/landing). Considering the characteristics of the dynamic change of the SOC over time parameters, this paper creatively transforms the relatively static priority factor (Wen and Huo, 2020; Zhang and Yang, 2018) into a comprehensive dynamic priority factor for flights. Flights with smaller priority factors have a higher priority in queuing optimization.

Specifically, the characteristic parameters of flight f have a direct impact on its priority. The state of charge, mission characteristics, the operation mode is represented as R_f, V_f, O_f, respectively. The priority of flight f at time t is $prior_f(t)$. According to the importance of the three characteristic parameters (SOC > mission characteristics > operation mode), the priority is calculated by using Eq. (34) (Wang et al., 2004).

Waiting for the aircraft in the queue at the junction to sort at a certain tailing interval, to ensure the fairness of flight priority calculation, the location node of the first aircraft as a reference to correct the power load status SOC_f^* (Eq. (30)). To prevent excessive discharge of the battery, 10% is considered a battery protection threshold (Kleinbekman et al., 2020). The power consumed by the path from the nearest and farthest boundary points to the vertiports is used as the level 1 priority boundary (Eq. (31)).

$$SOC_{fj}^* = SOC\left(st_f^j\right) - P_{sf}^j - 1\delta_{ff}, E_c \tag{30}$$

$$R_f(t) = \begin{cases} 1, & 16\% \leqslant SOC_{fj}^* < 32\% \\ 2, & 32\% \leqslant SOC_{fj}^* < 66\% \\ 3, & 66\% \leqslant SOC_{fj}^* < 100\% \end{cases} \tag{31}$$

$$V_f = \begin{cases} 1, & \text{Urgent tasks} \\ 2, & \text{Otherwise} \end{cases} \tag{32}$$

$$O_f = \begin{cases} 1, approach \\ 2, departure \end{cases} \tag{33}$$

$$prior_f(t) = PRIOR\left(R_f(t), V_f, O_f\right) = \frac{\left(pri_f(t) - 1\right)\left(pri_f(t) - 2\right)\left(pri_f(t) - 3\right)}{6} + \frac{\left(2pri_f(t) - R_f(t) - 2\right)\left(R_f(t) - 1\right)}{2} + V_f \tag{34}$$

And

$$pri_f(t) = R_f(t) + V_f + O_f$$

For example, if flight 1 is an approaching flight on an emergency mission and SOC_1^* is 25%, i.e.$R_1 = 1, V_1 = 1, O_f = 1$, then flight 1 has priority $prior_1 = PRIOR(R_1, V_1, O_1) = 1$. Similarly, a three-dimensional priority table for flights can be derived (Table1).

4. Description of the algorithmic process

The adaptive control strategy for the scheduling of approach-departure flights in MVS-TA includes two parts: the construction of the operating environment and operating rules, and the integrated adaptive scheduling model (Fig. 5). The specific process of the adaptive scheduling optimization part is as follows (Fig. 6):

(1) **Initialization of information parameters:** topology of the traffic network in the terminal area, allowed pass time (green time) for each phase of the first cycle, road traffic, road impedance, and basic information about the flight (including initial point, destination, initial power, mission characteristics., mode of operation, etc.).
(2) **Data update of the operating environment:** At the beginning of the tp cycle, update the segment traffic $QL_a(tp+1)$, junction green light ratio $\varphi_{p_i^k}(tp+1)$ of tp, as well as the segment impedance $w_{ij}(tp)$. At the end of the tp cycle, record the queue length $Q_a(tp)$ and segment traffic $QL_a(tp)$ of tp, and update the turn probability $R_{ab}(tp)$ according to the queuing data.
(3) **Minimum time path planning:**When a flight reaches each transit junction, with minimal impedance W_f as the optimization target, the Dijkstra algorithm is used to calculate the shortest-time path and determine the next junction and segment.

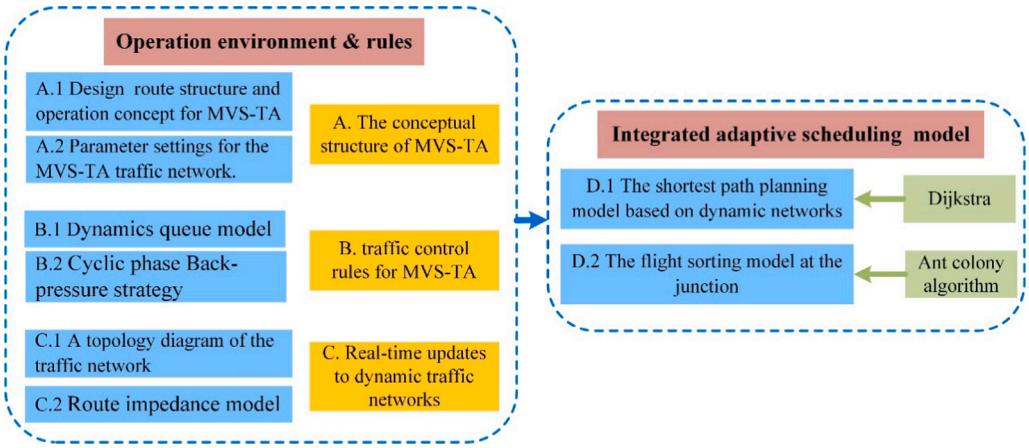

Fig. 5. The overall framework of the adaptive control strategy in MVS-TA.

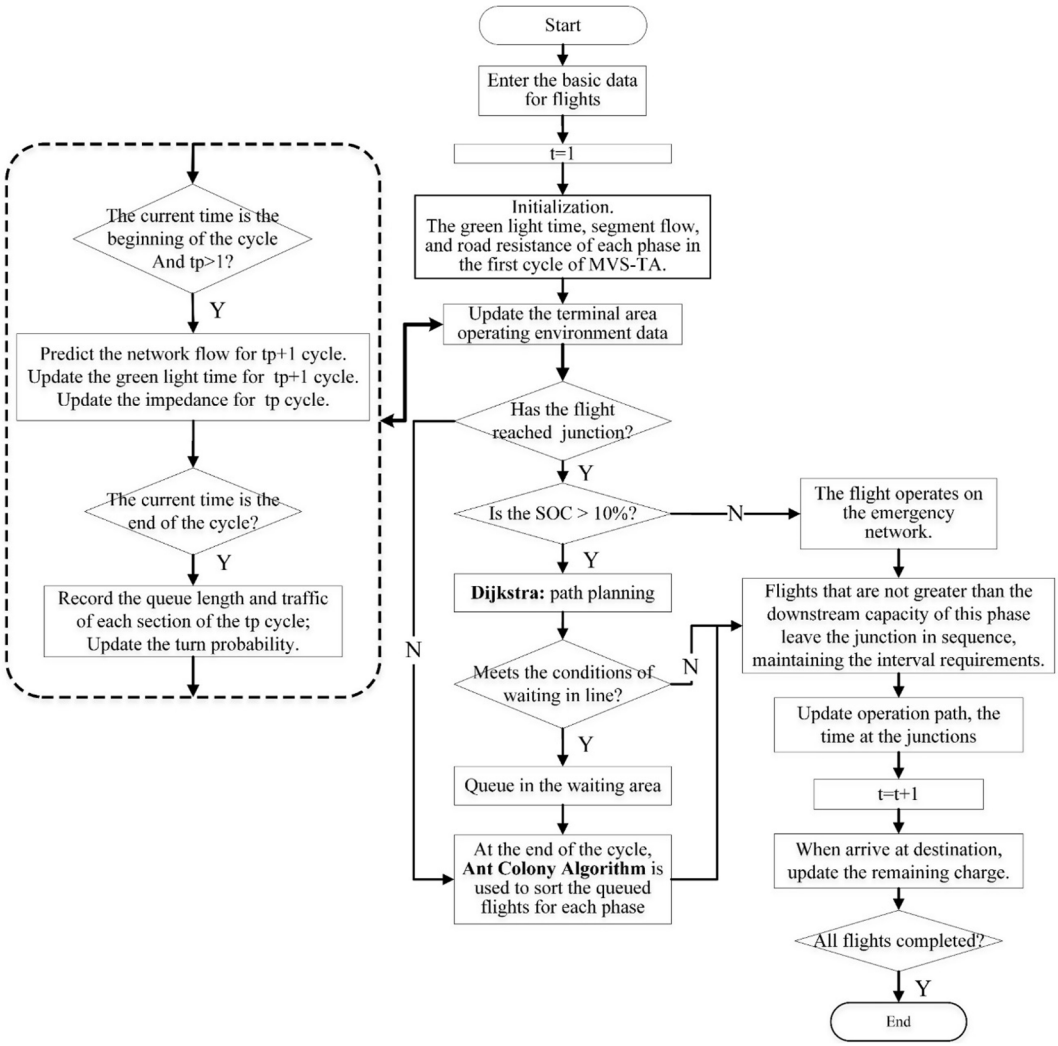

Fig. 6. The process of adaptive control strategy algorithm.

(4) **Waiting and sequencing at the junction:** Determine the phase that controls the passage of a flight based on the next running section updated. Flights with less than 10% of the remaining power are operating on the emergency ring. Flights that meet (29a) (29b) will need to be suspended waiting in line until the phase is allowed to pass. At the end of each cycle, to minimize the weighted time $Delay_f^j\left(st_f^j\right)$ through the junction, the Ant Colony Algorithm (ACO) is used to sort the queued flights so that the more important flights can pass through the junction first. The flight will continue to wait until the next cycle if the following occurs: 1) the optimized passage time of the flight exceeds the green pass time range of the phase. 2) The capacity of the next route to be remitted has reached the upper limit.

(5) **System scheduling judgment:** scheduling all flights introduced by the system. Exit scheduling when all flights have completed route planning and end the operation in the terminal area (approach flights arrive at the vertiports, departure flights leave the outer ring layer).

5. Numerical examples and result analysis

5.1. Experiment scenario settings

(1) **Aircraft-related parameter settings (see Table 2):** Take the Ehang 216, an aircraft with 16 propellers that can carry two people for experimental simulation, the cruise speed is 130 km/ h (about 36.1 m/s). In this paper, the cruising speed is set at 36 m/s, the horizontal speed $v_x = 8m/s$ at altitude drop (Stages (2)-(3) and (5)-(6) in Fig. 9), the vertical speed is variable. The speed of the vertical take-off and landing phase (stage (9)in Fig. 9) is 3 m/s, and assume that eVTOL can operate continuously for 1 hour (EHANG216, n.d.; Kleinbekman et al., 2018). (Cotton, 2019) studied the design separation values between multiple types of aircraft (manned/unmanned eVTOL, VFR/IFR/AFR, etc.) and concluded that the longitudinal interval between unmanned eVTOLs with passengers could be as low as 300ft. (Bosson and Lauderdale, 2018) use the spatial separation criteria of 0.3nmi and 100ft as simulation scenarios. Based on the above research, this paper sets the distance interval of 0.3nmi (about 555.6 m, interval of about 15 s) when the aircraft cruises, and calculates the maximum capacity of the route. Taking into account the FAA's interval requirements for F-class aircraft (less than 15,400 lb) (Bosson and Lauderdale, 2018; Federal Aviation Administration, 2016), this paper sets the time interval between the aircraft's sequencing at the junction and vertiport to 60 s, taking into account the complex operating scenarios of the junction.

By adjusting the proportion of the cruise stage (flying at cruising speed) during the down/climbing phase, the energy consumption of the eVTOL can be optimized and is conducive to the avoidance of high-rise buildings (Kleinbekman et al., 2018). In the experimental scenario settings, the proportion of the horizontal running phase of the flight at cruising speed is 60% of the drop/climb phase (for example, stage (2) in Fig. 9 accounts for 60% of the drop stage (2)–(3)).

(2) **The parameter settings for the operational environment (see Table 3 and 4):** The operating environment includes the setting of terminal area structure and control rules. An application structure of the conceptual structure of MVS-TA proposed in this paper can be constructed as shown in Fig. 7. According to (Bertram and Wei, 2020; Kleinbekman et al., 2018), setting the radius of $Ring_A$, $Ring_B$, and $Ring_C$ to 3500 m, 2000 m, and 600 m, respectively. The emergency ring layer has a radius of 1000 m, the same horizontal plane as $Ring_C$, and the vertical distance between the plane and the landing site is 200 m. The terminal area concept is converted into a traffic topology map for simulation, where the traffic path topology on the approach side is shown in Fig. 8. In practice, the parameters in the MVS-TA conceptual structure and control rules need to be adjusted according to the actual operating conditions.

Compared with the adaptive terminal area system, it is the traditional terminal area airspace structure applied to civil aviation (Fig. 10). To ensure the validity of the comparison results, the ring layer parameters and the position of the points of the traditional airspace structure are basically the same as between the adaptive terminal area structure, but there is no emergency ring layer. There are no points controlled by the signal light in the airspace structure. The approach- departure fixes are only distributed in the outermost ring layer.

(3) **The adaptive control system (ACS) and the traditional control system (TCS):** The implementation of ACS relies on the signal control based on the backpressure strategy and integrated adaptive model. The advantage is that the adaptive control and distributed control of the busy systems can be realized, the flight path and sequence can be optimized, and the flight with high importance can end the terminal area operation stage first.

Since civil airliners cannot hover during the voyage, if the terminal area is saturated, traditional air traffic management usually adopts the strategy of air and ground waiting to dispatch flights. Under the constraints of separation, sector capacity, runway usage separation, airport service capability, etc., the approach-departure flights are scheduled and sorted. The flights that are not authorized to enter (or leave) the terminal area are subject to waiting at the holding pattern (or airport). The characteristics of the traditional airspace structure and control strategy are that 1) there is a fixed route between the approach-departure fixes and the vertiport, and 2) the flight cannot change the route determined during the flight. Referring to the flight optimization study of civil aviation's regional multi-airport system (Shao et al., 2020; Zhang et al., 2017), the baseline model can be represented as Eq. (35)-Eq. 36.

Table 2
eVTOL operating parameters and separation settings.

Operation parameters				Cruising separation	Junction separation	Take-off and landing separation
Cruising speed	The speed at height drops	Vertical speed	Endurable time			
36 m/s	$v_x = 8$m/s, v_y variable	3 m/s	1 h	15 s	60 s	60 s

Table 3
Parameter Settings of adaptive control system.

Relevant parameters of transit junction		Vertiport capacity		
Time periodTP	Backpressure parameterη	Vertiport 1	Vertiport 2	Vertiport 3
120 s	40	20	20	20

Table 4
Parameter setting of traditional control system.

Sector capacity				Vertiport capacity			The separation at the junctions	Take-off and landing separation
Sector1	Sector2	Sector3	Sector4	Vertiport1	Vertiport2	Vertiport3		
30	25	25	25	20	20	20	60 s	60 s

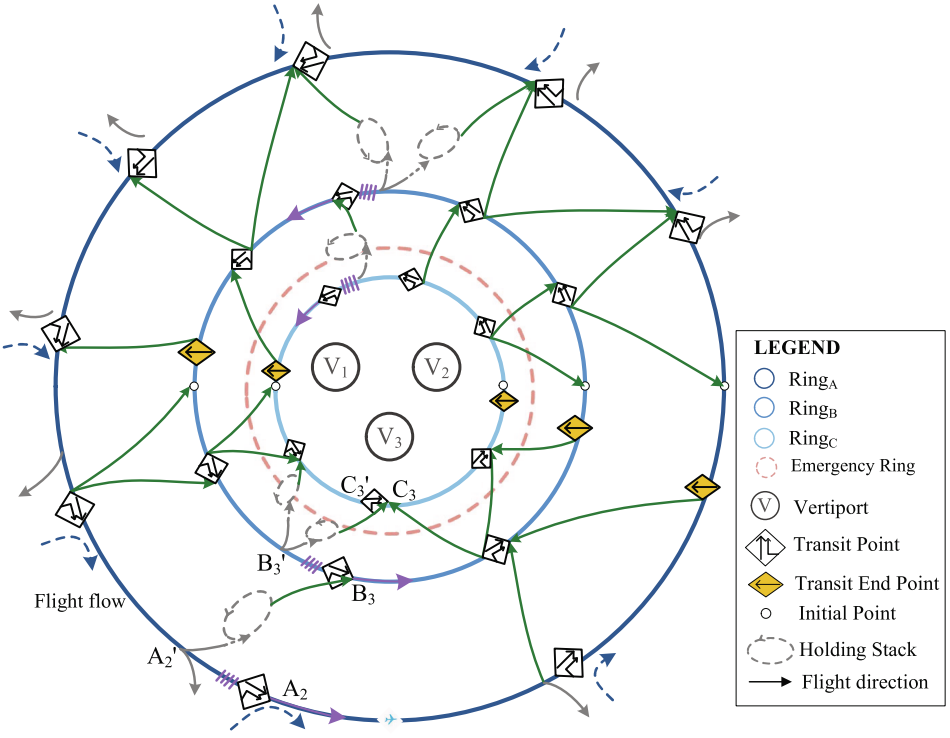

Fig. 7. Terminal area structure diagram of MVS.

$$min\left(\sum_{f\in F}\left(ET_f - ST_f\right)\right) \tag{35}$$

$$s.t.(FA_u(t), FD_u(t)) \in CR_u(t), \forall u \in U, \forall t \in T \tag{36a}$$

$$FS_s(t) \le CS_s(t), \forall s \in S, \forall t \in T \tag{36b}$$

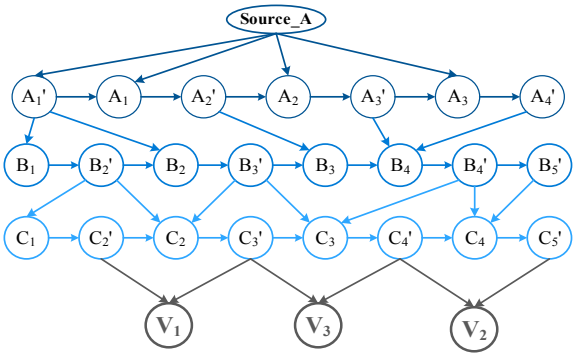

Fig. 8. The topology of the approach side traffic network.

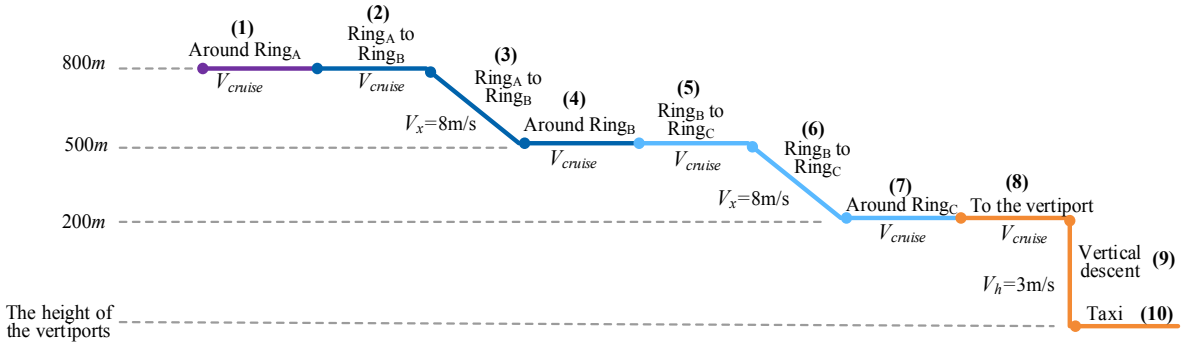

Fig. 9. Sectional view of the flight approach process.

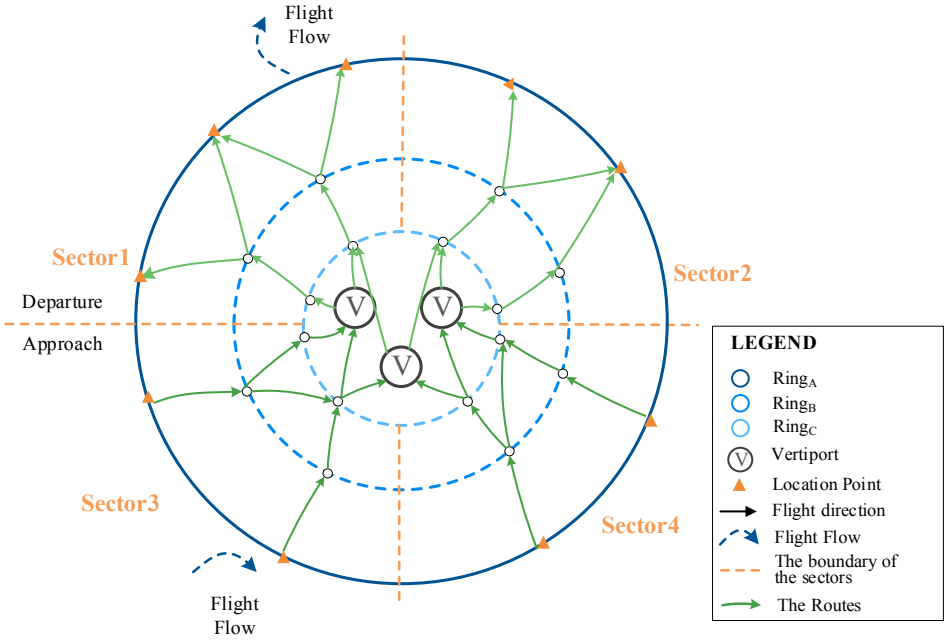

Fig. 10. Airspace structure of the traditional terminal area.

Table 5
Parameter settings in ACO.

Parameter	α	β	ρ	Q	Number of iterations
Value-ACS	1	5	0.3	100	300
Value-TCS	1	5	0.1	300	2500

$$w_{ff'}\rho_{ff'}\left(LPT_{f'}+\delta_{ff'}\right)\le LPT_f,\forall f,f'\in F \tag{36c}$$

$$\lambda_{ff'}\rho_{ff'}\left(ET_{f'}+\sigma_{ff'}\right)\le ET_f,\forall f,f'\in F \tag{36d}$$

$$ETA_f\le ET_f,\forall f\in F \tag{36e}$$

The optimization is to minimize the sum of all flight delays. ET_f and $ST_f$are the target runway time and estimated runway time of the flight f, respectively. Eq. (36a) are the vertiport capacity constraints, which mean that arrival flow $FA_u(t)$ and departure flow $FD_u(t)$ at the vertiport u during period t should meet the capacity constraint $CR_u(t)$. Eq. (36b) are the sector capacity constraints, which require that arrival-departure flights of the sector s during the period t ($FS_s(t)$)must satisfied the capacity $CS_s(t)$. Eq. (36c) ensure that the separation of the adjacent flight f and f', where $\delta_{ff'}$ represents the minimum safety separation. If flight f' is in the adjacent previous position of flight f, $\rho_{f,f'}$ is valued at 1, otherwise 0. If flight f and its previous flight f' are through the same location, $w_{ff'}$ value is 1, otherwise 0. Similarly, the Eq.(36d) is the separation constraint at vertiport u, where $\sigma_{ff'}$ represents the minimum safety separation and ET_f is the landing/take-off time of flight f. If flight f shares the same vertiport with f', $\lambda_{ff'}$ is valued at 1, otherwise it is 0. Eq. (36e) are time window constraints, which mean that the target runway time (ET_f) is greater than the minimum boundary (time to reach the system) ETA_f.

(4) **Parameter setting of ACO:** In this paper, the ACO is used to solve two problems, one is the optimization of queued flights at the intersection of ACS, and the other is the sorting of flights under TCS, that is, the baseline problem. Based on the general ACO, the algorithm used in this paper gives priority to low-power flights in each iteration and retains the optimal solution to the next iteration. According to (Duan, 2005), the best experience of parameter settings in the Ant-Cycle model of ACO is as follows:$0\le\alpha\le 5; 0\le\beta\le 5; 0.1\le\rho\le 0.99; 10\le Q\le 10000$.

The parameter of ACO in this paper are set according to the experience of research (Duan, 2005) (Wu et al., 2016), see Table 5.

5.2. Results analysis

To validate the performance of the proposed MVS-TA structure and scheduling strategy, a computational study based on a variety of scenarios was carried out and the results are presented in this section. In section 5.2.1, the performance of ACS and TCS is compared. In section 5.2.2, the effect of the characteristics of flight entry into the terminal area on ACS operating performance is explored. Section 5.2.3 further analyzes the performance of ACS in random arrival scenarios. Given the actual application scenario, approach flights are about 1.5 times the number of departure flights, and the demand of the three vertiports is relatively evenly distributed.

It should be noted that: 1) The time that eVTOL enter the terminal area (ETA) refers to the arrival of the approach-flight to the outer ring boundary or departure flight ready to take off. 2) The end of the terminal area operation phase refers to the arrival of approaching flights to the vertiport or departure flights leaving the outer ring layer of the terminal are. 3) The flight entry interval reflects the density of the flight to be sorted.

5.2.1. Performance of ACS and TCS for multi-vertiport

To compare the performance of the two systems with different terminal area structures and control strategies, this paper sets up an instance scenario with the flight volume to be sorted as 10/20/…/100, and assumes that ETA intervals are subject to the Poisson distribution of $\lambda = 60$. The initial power of approaching flights is normally distributed with an average of 35% and a standard deviation of 5%, while the initial power of departure flights is normally distributed with an average of 92% and a standard deviation of 2.5%. The calculation of ACS and TCS is based on the algorithm framework (Fig. 6) and ACO, respectively. Fig. 11 shows the average flight time of TCS in scenarios where the number of flights is 20 and 40, with a maximum difference of 14.82% and 28.70%, respectively. Therefore, when comparing the two strategies, the data obtained by TCS is an average of 10 simulations.

Select the operation data with the number of flights to be sorted as 20, 50, 80, 100 respectively for preliminary analysis (In TCS, select the set of flight operation data that is closest to the average). When the number of flights to be sorted is 20 (NumF = 20), the slope of flights leaving the terminal area overtime under TCS is slightly greater than that under ACS, i.e. the number of flights leaving the terminal area in unit time under TCS is higher and the operating efficiency is higher (Fig. 12a). With the increase in the number of arrival flights, the number of flights stranded in MVS-TA under TRS increased (i.e., the operation time of each flight increased), the gap between the two control strategies operating efficiency gradually increased, the advantages of ACS became more and more obvious. The maximum gap in the number of stranded terminal flights was 16, 23, and 38, respectively, in NumF-50/80/100. (Fig. 12b, 12c, 12d).

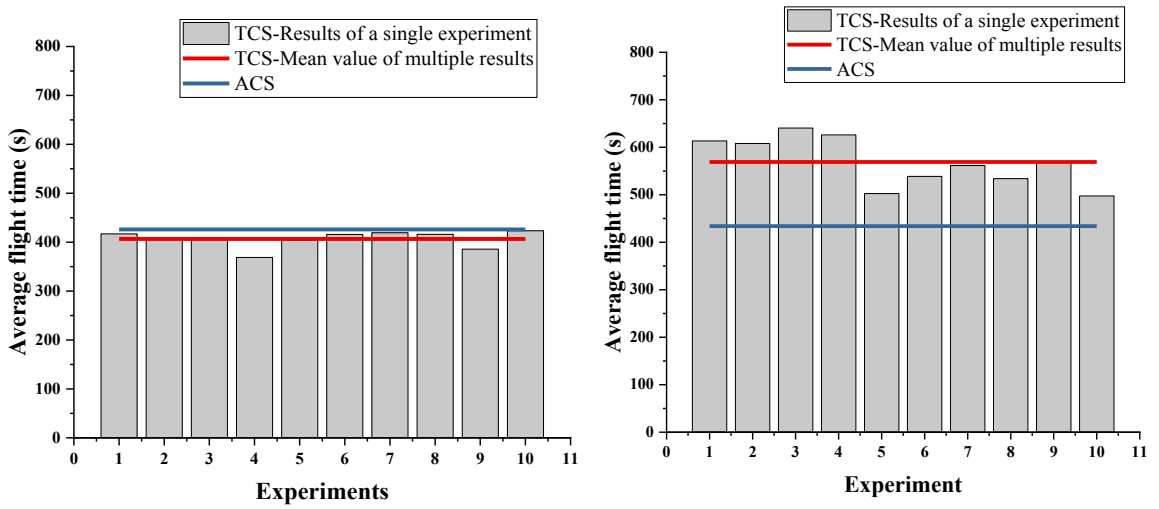

a. Average flight time in MVS-TA in NumF=20 b. Average flight time in MVS-TA in NumF=40

Fig. 11. Multiple result data under TCS in NumF = 20 and NumF = 40 (Note: Average flight time: In the corresponding simulation case, the average flight time of several flights in the terminal area).

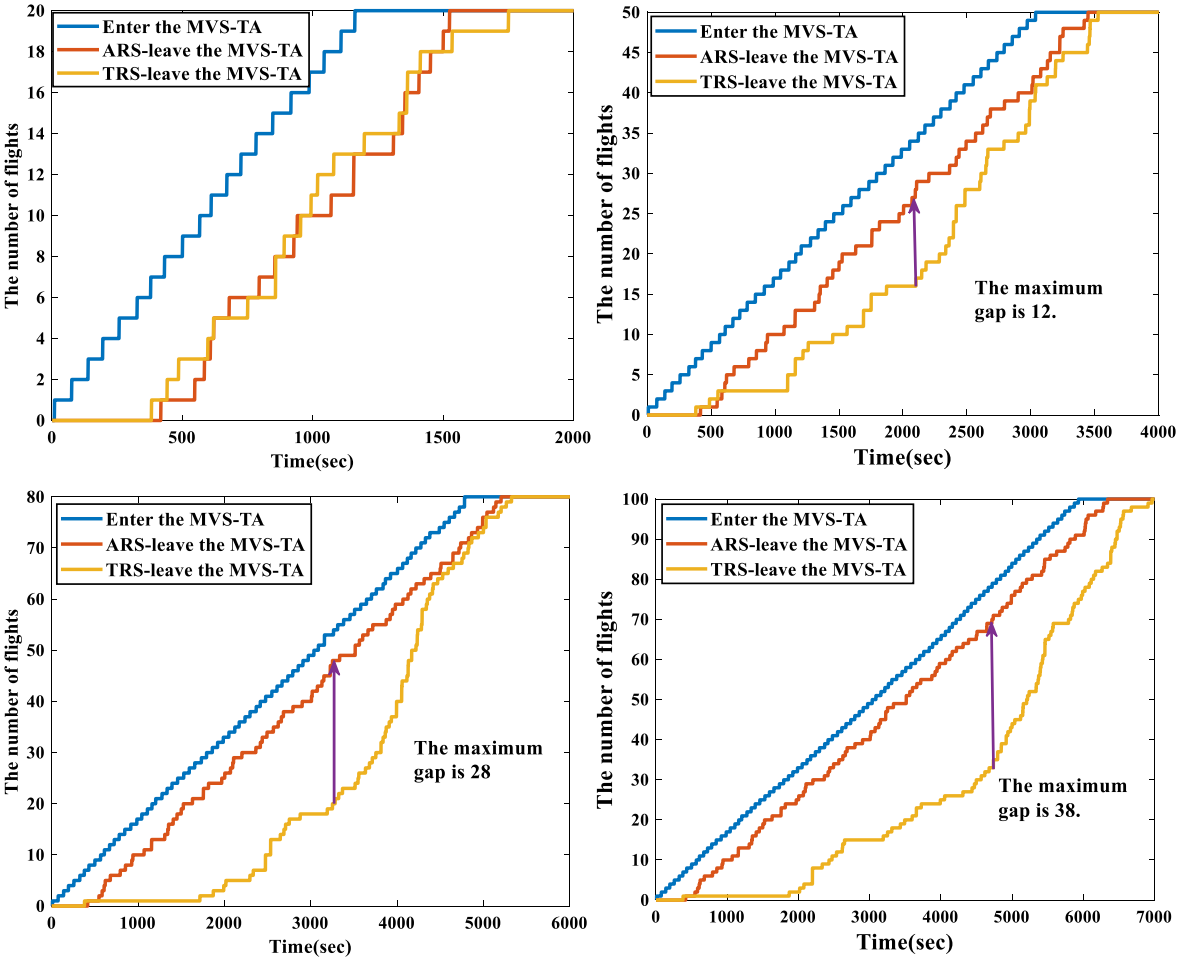

Fig. 12. The cumulative number of flights leaving MVS-TA over time under the ACS and TCS. (a) NumF = 20; (b) NumF = 50; (c) NumF = 80; (d) NumF = 100.

Table 6
Comparison of flight operation data under ACS and TCS.

Flights	Average flight time			Standard deviation		Average power consumption			Danger separation		Power alarm	
	ACS	TCS	Gap	ACS	TCS	ACS	TCS	Gap	ACS	TCS	ACS	TCS
10	409.5	406.35	**−0.8%**	87.1	160.9	0.1107	0.1110	−0.1%	1	0	0	0
20	426	406.58	**−4.6%**	78.3	100.4	0.1172	0.1093	−6.7%	2	1.2	0	0
30	431.57	473.66	9.8%	76.8	230.8	0.1191	0.1286	8.0%	3	1.1	0	0
40	433.98	568.92	31.1%	73.9	335.6	0.1199	0.1551	29.4%	3	3.3	0	0.3
50	435.9	791.98	81.7%	78.2	552.2	0.1176	0.2154	83.2%	4	6.3	0	1.9
60	436.43	943.74	116.2%	80.3	779.9	0.1189	0.2505	110.7%	4	12.8	0	2.5
70	438.66	1130.08	157.6%	78.7	934.4	0.1161	0.3064	163.9%	4	8.1	0	**16.4**
80	436.64	1372.89	214.4%	74.8	1141.4	0.1164	0.4041	247.3%	5	11.2	0	**23.7**
90	439.66	1599.66	263.8%	73.8	1375.1	0.1179	0.4521	283.5%	5	17.2	0	**31.1**
100	441.08	1845.36	318.4%	77.5	1524.1	**0.1164**	**0.4978**	327.7%	7	17.3	0	**41.3**

Note: 1) Average flight time: under the corresponding control strategy, average operation time in MVS-TA for each flight in each case. 2) Average power consumption: under the corresponding control strategy, the average power consumption per flight in the MVS-TA (The remaining electricity of the flight is calculated according to Eq. (28)). 3) Danger separation: when the interval between two flights through the conflict point (conflict port) is less than 20 s (threshold), the alarm is triggered. The statistics in the table are the total number of times the alarm was triggered in the experimental scenario. 4) Power alarm: If the charge of the flight is less than 0 during the operation, the electricity alarm will be triggered. The statistics in the table are the total number of electricity alarms triggered in the simulation.

Further, from the perspective of operational efficiency and safety level, the difference between the two control strategies is explored. The simulation data of each scenario are shown in Table 6.

Operation efficiency: With the increase in the number of flights to be sorted, the Average flight time of flights under ACS increases slightly (less than7.71%) and stabilized overall, while under TCS there are significant fluctuations. The average operating time of NumF = 10 and NumF = 20 under TCS is 0.8% and 4.6% lower than that of ACS, respectively. The control performance of TCS is slightly better than that of ACS with a low number of flights. The control advantage of ACS is very obvious when the number of flights increases gradually (Fig. 13 a, b). Combined with Fig. 12, when the flight enters the terminal area at intervals of about 60 s, ACS can keep the number of flights staying in MVS-TA stable and low, ensuring the effectiveness and efficiency of scheduling.

Safety level: The average power consumption of the flights in the terminal area is positively related to the Average flight time. The average power consumption of the flights under ACS is 0.11–0.12, which is in a stable and acceptable range. Relatively speaking, when the number of flights to be sorted is 80, the average power consumption of TCS has reached 0.4041, which is more than 3 times that of ACS, and has exceeded the initial power average (0.35) set by the approach-flight experiment. When the volume of flights to be sorted is further increased to 100, the average power consumption of the flights under TCS is as high as 0.4978, which is about 4.3 times that of ACS. In the experimental scenario of NumF = 70/80/90/100, due to the long time of flights under TCS in the terminal area, 16.4 (23.4%), 23.7 (29.6%), 31.1 (34.6%) and 41.3 (41.3%) flights respectively ran out of power, triggering the power alarm. This situation is undoubtedly a fatal risk for eVTOL, which uses electricity as the only power source. In addition, this paper puts forward the " Danger separation alarm" as an indicator to compare the two control systems in terms of safety: The distance between the innermost ring layer of the MVS-TA and vertiports is short, and it has the characteristics of small airspace range and complex route structure, which is more likely to produce danger separation than other ring layers. In this paper, the eight points in the innermost layer of the traditional airspace structure are set to the monitoring points of the danger separation alarm. The ten junctions in the innermost layer of the MVS-TA are set to the monitoring points of the alarm. A conflict alarm is triggered when two flights pass through the conflict point (conflict port) for less than the threshold. When the number of flights to be sorted is greater than 40, the number of danger separation alarms

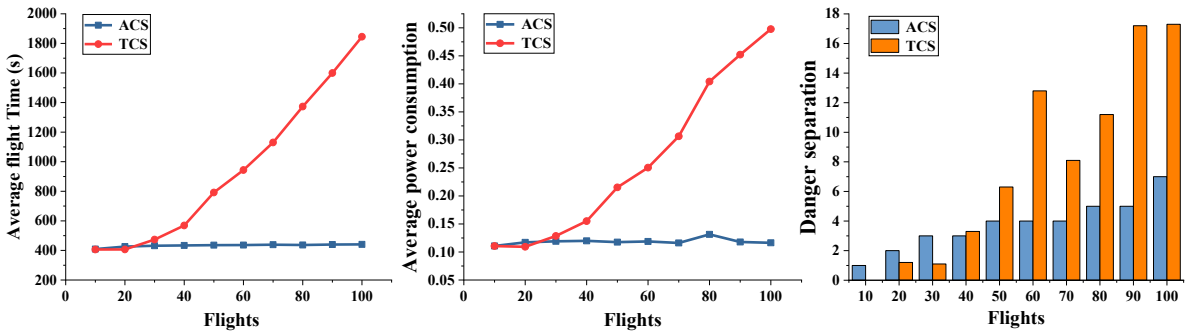

Fig. 13. TCS and ACS performance comparison (a) the average flight time of each flight in the MVS-TA (b) average power consumption (c) the number of danger separation alarms.

under TCS is higher than ACS (Fig. 13c).

It should be noted that (Vincent et al., 2018) suggests that the DWC (Detect and Avoid Well-Clear) definition of terminal airspace should define vertical intervals of 450ft, HMD (Horizontal Miss Distance) should be 1000ft-2000ft, and τ should be 15sec-25sec. For this reference, this section sets the threshold for danger separation alarm to 20sec.

Due to the limitations of TCS, the number of flights accommodated in the terminal area is lower than the adaptive terminal area structure. When the number of flights increases and cannot land in the vertiport (or leave the terminal area) in time, the operation time will increase. TCS only limits the time separation through the approach-departure fixes, and can not control the other junctions. The increase in the number of flights and flight density will bring an unacceptable risk of danger separation. Relatively speaking, when the ETA intervals are subject to the Poisson distribution of λ=60, the performance of ACS is relatively stable, and the average flight time and average power consumption are at a low level.

It should be noted that although the number of danger separation alarms under ACS also has a slight increase with the increase in flight volume, the design and rules of the concept structure itself greatly reduce the probability that flight danger separation will lead to conflict. Most junctions in the conceptual structure include shadow nodes (flights can only be remitted out of the ring layer, no signal light control) and control nodes (signal control nodes). The structure can guarantee the separation (60 s) of the flight through the control node. Because the shadow node of the same intersection is close to the control node, the danger separation alarms can also be triggered if the interval between two flights through the same intersection is less than 20 s. This is the source of most danger separation alarms in ACS and is the main reason why alarms still exist in low flight volume cases. It is worth noting that the flight routes at these two points are different, and the possibility of danger has been greatly reduced.

5.2.2. The impact of flight characteristics on ACS operating performance

Experiment 1 has proved the efficiency and safety of ACS relative to TCS. ACS guarantees the stability of the flight's running time and power consumption in the terminal area when the ETA intervals are subject to the Poisson distribution of $\lambda = 60$. Experiment 2 will continue to explore the impact of flight volume and flight entry interval (flight density) on the operational performance of ACS.

The intervals between the time of flight entering MVS-TA (ETA) are set to obey the Poisson distribution of $\lambda = 60, \lambda = 40, \lambda = 30, \lambda = 20$ respectively. For the same ETA interval, different flight volumes are set. The simulation cases are shown in Table 7.

The number of flights stranded in the terminal area at a given time is the difference between the cumulative number of flights entering and leaving the terminal area at that time. When the ETA interval is gradually reduced (the density of flights to be sorted increases), the continuous flight into the terminal area increases the system load, so that the delay time and average running time increase due to the increase of the queue length of the junction. The flight that cannot reach the destination in time will always run in the route network, so the number of flights stranded in the terminal area at every moment is increasing. With the increase in the number of flights, the number of flights stranded in the terminal area at each time in SCE1/SCE2/SCE3 (ETA-interval average is 60 s/40 s/30 s) remains volatile and stable, with the upper limit remaining at 10/15/20, respectively. However, there has been a marked increase in the number of flights stranded at various times in SCE4, which is 1.65 times, 1.95 times, 2.4 times, 2.7 times that of SCE3, respectively (Fig. 14).

From the point of view of system **efficiency**: **1)** When the average ETA interval of 60 s/40 s/30 s (the density of the flight to be sorted is small) and unchanged, the average flight time increases with the increase in the number of flights, but the fluctuation is small (2%-7%). When the average ETA interval is 20 s, the average flight time increases significantly as the number of flights increases

Table 7
Experimental cases.

	Scenario	The number of flights to be sorted (NumF)	ETA interval.	Initial electricity
SCE1	SCE1-1	50	$\lambda = 60$Poisson Distribution	The initial electricity of approaching flights is subject to $N(0.35, 0.05^2)$
	SCE1-2	100		
	SCE1-3	150		
	SCE1-4	200		
	SCE1-5	250		
SCE2	SCE2-1	50	$\lambda = 40$Poisson Distribution	
	SCE2-2	100		
	SCE2-3	150		
	SCE2-4	200		
	SCE2-5	250		
SCE3	SCE3-1	50	$\lambda = 30$Poisson Distribution	The initial electricity of departing flights subject to $N(0.92, 0.025^2)$
	SCE3-2	100		
	SCE3-3	150		
	SCE3-4	200		
	SCE3-5	250		
SCE4	SCE4-1	50	$\lambda = 20$Poisson Distribution	
	SCE4-2	100		
	SCE4-3	150		
	SCE4-4	200		
	SCE4-5	250		

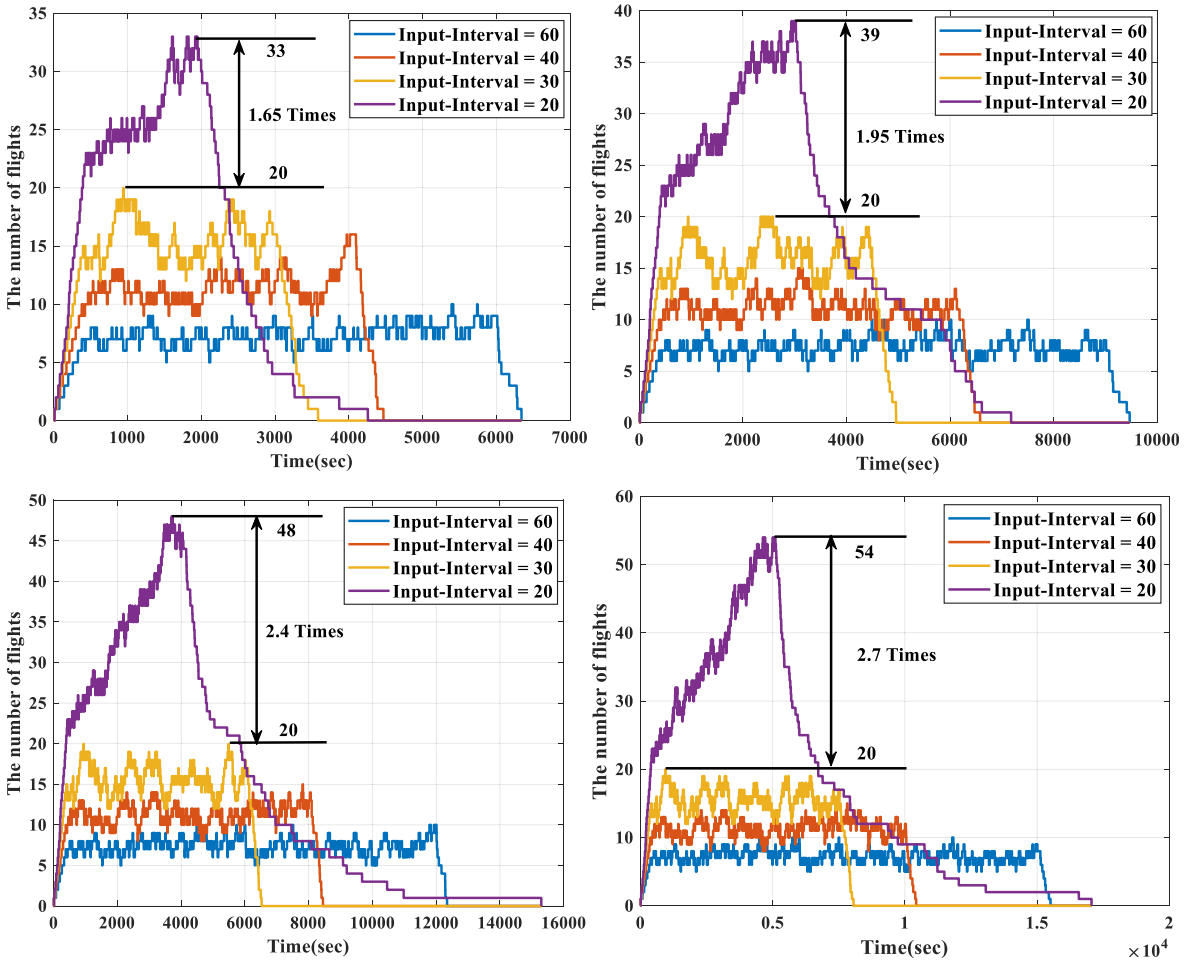

Fig. 14. Number of flights stranded in the terminal area under ACS (a) NumF = 100 (SCE1-2/ SCE2-2/ SCE3-2/ SCE4-2) (b) NumF = 150 (SCE1-3/ SCE2-3/ SCE3-3/ SCE4-3); (c) NumF = 200 (SCE1-4/ SCE2-4/ SCE3-4/ SCE4-4); (d) NumF = 250 (SCE1-5/ SCE2-5/ SCE3-5/ SCE4-5).

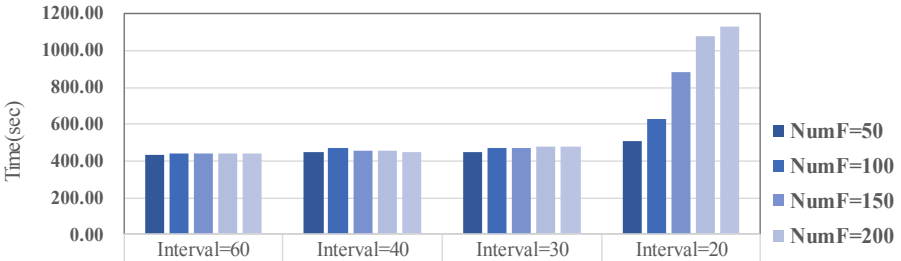

	Interval=60	Interval=40	Interval=30	Interval=20
NumF=50	435.90	451.80	450.80	508.70
NumF=100	441.08	468.31	474.21	627.78
NumF=150	442.22	456.60	474.65	885.12
NumF=200	443.01	457.24	476.02	1074.37
NumF=250	440.36	452.22	480.44	1130.60

Fig. 15. Average flight time in the terminal area.

Table 8
Simulation result data.

Flights		50	100	150	200	250
Average flight time (s)	A = 60 (SCE1)	435.9	441.08	442.22	443.01	440.36
	A = 40 (SCE2)	+3.6%	+6.2%	+3.3%	+3.2%	+2.7%
	A = 30 (SCE3)	+3.4%	+7.5%	+7.3%	+7.5%	+9.1%
	A = 20 (SCE4)	+16.7%	+42.3%	+100.2%	**+142.5%**	**+156.7%**
Average power consumption	A = 60 (SCE1)	0.1176	0.1164	0.1186	0.1195	0.1168
	A = 40 (SCE2)	+1.1%	+6.9%	+0.9%	+2.1%	+3.5%
	A = 30 (SCE3)	+1.4%	+10.8%	+7.8%	+8.5%	+11.6%
	A = 20 (SCE4)	+16.4%	+47.3%	+104.6%	**+139.7%**	**+157.7%**
Average number of hovers	A = 60 (SCE1)	1.3	1.26	1.17	1.2	1.2
	A = 40 (SCE2)	1.1	1.13	1.15	1.08	1.11
	A = 30 (SCE3)	1.1	1.25	1.21	1.19	1.22
	A = 20 (SCE4)	1.3	1.85	2.35	2.56	2.74
Average hover time (Average delay time) (s)	A = 60 (SCE1)	78.26	79.83	81.04	80.28	78.72
	A = 40 (SCE2)	93.8	109.55	95.13	94.7	90.99
		+19.9%	+37.2%	+17.4%	+18.0%	+15.6%
	A = 30 (SCE3)	94.16	118.75	114.57	113.71	120.93
		+20.3%	+48.8%	+41.4%	+41.6%	+53.6%
	A = 20 (SCE4)	151.66	280.43	**538.64**	**730.86**	**789.46**
		+93.8%	+251.3%	**+564.7%**	**+810.4%**	**+902.9%**
Power alarm	A = 60 (SCE1)	0	0	0	0	0
	A = 40 (SCE2)	0	0	0	0	0
	A = 30 (SCE3)	0	0	0	0	0
	A = 20 (SCE4)	0	1	14	**23**	**30**

Note: The percentage of the line of SCE2, SCE3 and SCE4 indicates the **gap** between the data of this case and that of SCE1.

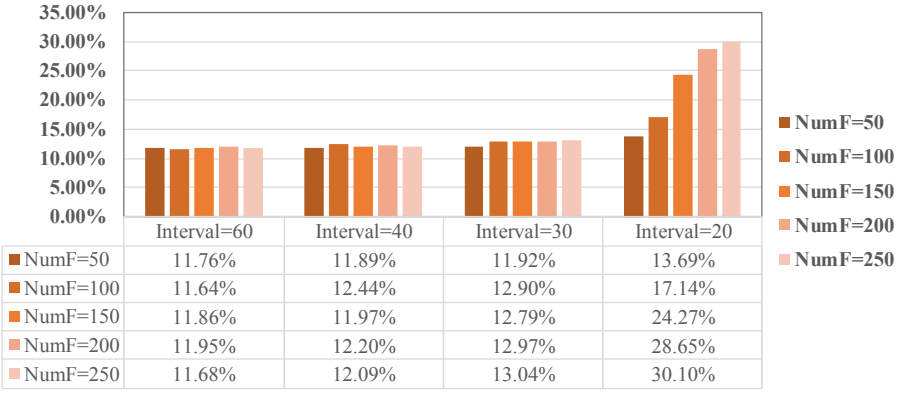

	Interval=60	Interval=40	Interval=30	Interval=20
NumF=50	11.76%	11.89%	11.92%	13.69%
NumF=100	11.64%	12.44%	12.90%	17.14%
NumF=150	11.86%	11.97%	12.79%	24.27%
NumF=200	11.95%	12.20%	12.97%	28.65%
NumF=250	11.68%	12.09%	13.04%	30.10%

Fig. 16. The average power consumption of the flight in the terminal area.

(Fig. 15), and the average hover time (average delay time) is similar to the trend of the Average flight time. **2)**When the number of flights is certain, with the increase of the density of flights to be sorted, the average flight time, average delay time and other indicators have also increased (Fig. 15, Table 8), especially in the case of ETA intervals of 20 s and high flight volume. Compared to SCE1 (Baseline), the average flight time of SCE2 and SCE3 in the same flight volume increased by 3%-7% and 3%-10%, respectively, while the operational efficiency of the terminal area in SCE4 was greatly reduced. The average operating time increased by 16%-157% in SCE4, and the average delay time in SCE4-3/SCE4-4/SCE4-5 was about 6.7 times, 9.1 times and 10 times the baseline, respectively.

From the point of view of system **safety**, the average power consumption of the flight in the terminal area is positively related to the average running time. In SCE1/SCE2/SCE3 (ETA interval average is 60 s/40 s/30 s), the average amount of electricity used increases

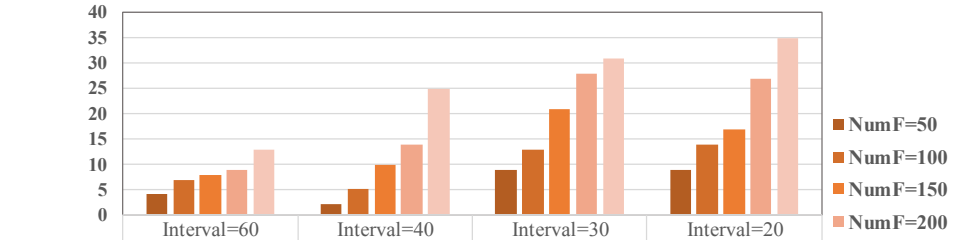

	Interval=60	Interval=40	Interval=30	Interval=20
NumF=50	4	2	9	9
NumF=100	7	5	13	14
NumF=150	8	10	21	17
NumF=200	9	14	28	27
NumF=250	13	25	31	35

Fig. 17. The cumulative number of alarms at the conflicting ports.

slightly with the number of flights or the density of flights, but no amount of flights is running out of power. In SCE4 (when the ETA interval average is 20 s), the average power consumption of flights increased significantly with the increase in flight volume (Fig. 16), with SCE4-4 and SCE4-5 having 23 (11.5%) and 30 (12%) power alarms, respectively (Table 8). On the one hand, as the number of flights increases, the number of danger separation in SCE1/SCE2/SCE3/SCE4 increases. Since the average ETA interval in SCE4 is 20 s, equal to the conflict threshold (20 s), there is a significant increase in the number of dangerous separations in SCE4 (The number of danger separation in NumF = 250 is about 2.89 times higher than that in NumF = 50, Fig. 17). On the other hand, the number of danger approaches increases with the increase of flight density. As described in 5.2.1, although the number of danger approaches increases with the increase of flight volume, the probability of collision can be greatly reduced because the operation directions of shadow nodes and control nodes are different.

5.2.3. ACS performance in random demand scenarios

Considering the characteristics of UAM's air transport service in practice, the time of flights entering the terminal area may be random. Experiment 3 sets different number of flights to be sorted during the same period time (1 h). The ETA is random, i.e. there may be a situation where a flight of the same/different route enters the terminal area at the same time. The ETA is a random number of [1, 3600]. The average interval of ETA in simulation cases are shown in Table 9. The initial power of the approach flights is subject to the normal distribution$(0.35, 0.05^2)$, and the initial power of the departure flights is subject to the normal distribution $(0.92, 0.025^2)$. The number of approach flights is 1.5 times the number of departure flights.

Overall, with the increase in the number of FIM per hour, the average operating time and average delay time of each flight increased relatively small when the flight density was 100/hour and 150/hour. The increase in these two indicators increased significantly as the flight density continued to increase (Fig. 18). When the flight density is 2 times that of the baseline scenario, the average operating time and average power consumption of flights in SCE5-2 increased by less than 7%, and the total scheduled operation time increased by only 3.0% (Table 10). When the flight density is three times that of the baseline scenario, the average flight time and average power consumption in SCE5-3 increased by 12.4% and 12.0%, respectively, and the total operation time increased by less than 5%. There is no alarm of flight power exhaustion in SCE5-1/SCE5-2/SCE5-3. In the SCE5-4 and SCE5-5 scenarios, the flight density into the MVS-TA within 1 h is four and five times that of the baseline scenario, respectively. The average flight time of SCE5-4 and SCE5-5 increased significantly, by 59.3% and 50.7%, respectively, of which the total operation time of SCE5-5 was approximately 1.5 times that of SCE5-1. Besides, 9 aircrafts (4.50%) and 21 aircrafts (8.40%) triggered the power alarm, and the safety level was

Table 9
The average interval of ETA for random demand scenarios.

Scenario	Frequency	Average interval of ETA (s)
SCE5-1	50 flights/hour	67.20
SCE5-2	100 flights /hour	35.24
SCE5-3	150 flights /hour	23.79
SCE5-4	200 flights /hour	17.81
SCE5-5	250 flights /hour	14.37

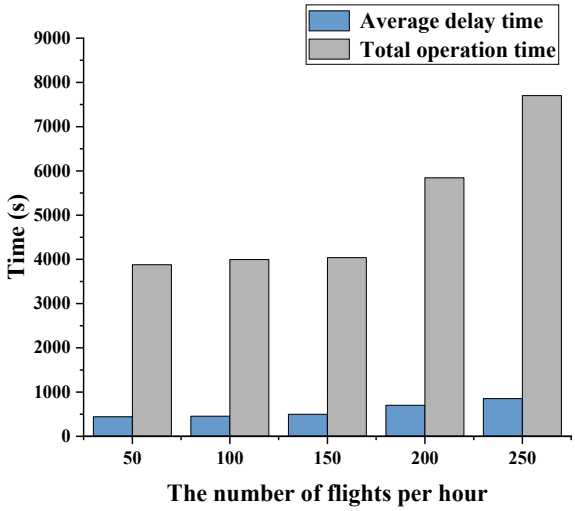

Fig. 18. Average flight time and average delay time for flights in ACS.

reduced to a certain extent.

Specifically, as flight density increases, ACS can increase the number of flights that end the terminal operation phase per unit time through effective scheduling (Fig. 19). When the frequency of entry to the MVS-TA is 50/100 (NumF = 50/hour, NumF = 100/hour), due to the large average interval of ETAs (67.20 s/35.24 s, respectively, Table 9), the number of flights stranded at each time in the terminal area is not greater than 20 and the operation is stable. When NumF grows to 200 or 250 per hour, the system is unable to schedule flights to the destination in time due to the small intervals between ETAs (17.81 s and 14.37 s, respectively). Therefore, the number of flights stranded in the terminal area always has increased significantly, and in the SCE5-5 scenario the value has reached 67 (Fig. 20) at t = 3067. This is why the Average flight time, the average power consumption increased greatly, and the operating efficiency and safety level of the MVS-TA decreased significantly.

Table 10
Results data for ACS in random demand scenarios.

Case		Average flight time (s)	Average power consumption	Total operation time (s)	Average delay time (s)
SCE5-1	50/hour	443.4	0.1179	3879	86.2
SCE5-2	100/hour	455.35 (+2.7%)	0.1260 (+6.9%)	**3995 (+3.0%)**	97.06 (+12.6%)
SCE5-3	150/hour	498.17	0.132	4040	140.71
		(+12.4%)	(+12.0%)	(+4.2%)	(+63.2%)
SCE5-4	200/hour	**701.56**	**0.1878%**	**5845**	357.13
		(+58.2%)	**(+59.3%)**	**(+50.7%)**	(+314.3%)
SCE5-5	250/hour	**853.27**	**0.2269**	**7703**	515.29
		(+92.4%)	**(+92.4%)**	**(+98.6%)**	(+497.8%)
Case		The average TL interval of the system (s)	Average number of hovers	Danger separation	Power alarm
SCE5-1	50/hour	222.32	1.16	3	0
SCE5-2	100/hour	119.79	1.25	11	0
SCE5-3	150/hour	77.15	1.73	19	0
SCE5-4	200/hour	**58.07**	1.33	23	**9(4.50%)**
SCE5-5	250/hour	**61.04**	1.5	**41**	**21(8.40%)**

Note: (1) The percentage of the line of SCE5-2, SCE5-3, SCE5-4 and SCE5-5 indicates the gap between the data of this case and that of SCE5-1. (2) The average TL interval of the system represents the average take-off and landing intervals of the three airports in the system. The smaller the value, the higher the ACS efficiency in the corresponding case.

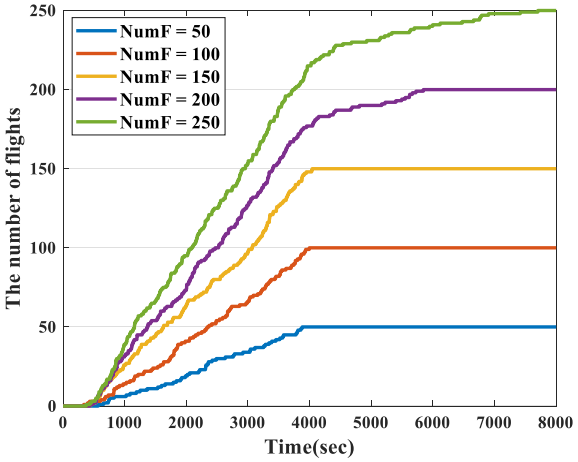

Fig. 19. The cumulative number of flights leaving the terminal area at each time.

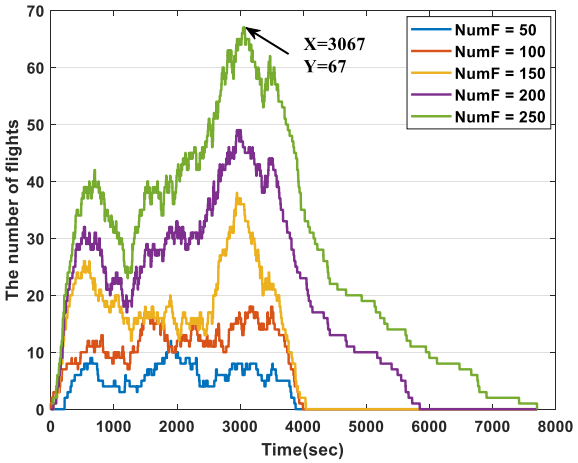

Fig. 20. Number of flights stranded in the terminal area.

6. Conclusion

This paper creatively proposes a set of adaptive control system for MVS-TA, including the concept of multi-ring structure, transit junction control rules, and flight integrated scheduling model. Under the similar terminal area route structure, set up a multi-group experiment with equal flight interval and different flight volume, and compare the ACS with the TCS. In addition, different flight scenarios are set to analyze the main factors affecting ACS.

The conclusions can be drawn by ACS compared with TCS: **1)** When the average interval between ETAs is at normal levels (60 s) and flight volumes are low (10 or 20), the control performance of TCS is slightly better than that of ACS. As the number of flights increases, ACS's control advantages become more prominent, with the average flight time under TCS already up to 4.2 times that of ACS when NumF is 100. **2)** When the average flight arrival interval is 60 s, with the increase of flight volume, the average power consumption of flights under ACS remains at 0.11–0.12, no power alarm. The maximum average power consumption under TCS is 0.4978, which is about four times that of TCS, and up to 40% of flights are alarmed. One of the major tasks of UAM is commuter flights. TCS is relatively unable to meet the operational requirements of the peak hours, and ACS is obviously more able to meet the operational efficiency and reliability of UAM.

Besides, based on the analysis of the experimental data of ACS, the following conclusions can be drawn: **1)** Flight arrival density has a greater impact on system recovery efficiency and safety levels than flight volume. When flight density does not meet the system tolerance limit, ACS's operational performance decreases only slightly as the number and density of flights increase (the density $\leq$ 120 flights/hour, the reduction less than 10.3%; the density $\leq$ 90 flights/hour, the reduction less than 7.5%). ACS can carry out flight scheduling and optimization through effective operation structure and strategy, so that MVS-TA can maintain high efficiency and safety. **2)** In the case of random flight entry, ACS can guarantee operational efficiency and safety level stability at flight density of fewer than 150 flights/hour. With the increase of flight density, the time of flight stranded in the terminal area gradually increases, and the

operational efficiency decreases. The ACS proposed provides a kind of airspace design for the future development stage of UAM, which can ensure the stability, adaptability, safety, and efficiency of MVS-TA operation.

The complete adaptive control system proposed in this paper can provide an important reference for the structural design and flight scheduling of MVS-TA in UAM. At the same time, the transit intersection control rules and the integrated scheduling model based on a dynamic route network can also be applied to the control scheduling of UAM urban airspace routes. The future research direction is to study the route structure and control rules of UAM in-depth and explore the influence of many factors on operational efficiency and safety performance. Also, explore the uncertainty factors of scheduling optimization to improve the robustness of the model application.

The simulation code for ACS is available at "https://github.com/Amelia55/Adaptive-Control-System-for-UAM".

Declaration of Competing Interest

The authors declare that they have no known competing financial interests or personal relationships that could have appeared to influence the work reported in this paper.

Acknowledgement

This is work was supported by the National Key R&D Program of China (grant no. 2018YFC0809500), the National Natural Science Foundation of China (grant no. 71874081), and Qing Lan Project of Jiangsu Province of China: 2020.

References

Bertram, J., Wei, P., 2020. An Efficient Algorithm for Self-Organized Terminal Arrival in Urban Air Mobility 1–10. Doi: 10.2514/6.2020-0660.

Bosson, C.S., Lauderdale, T.A., 2018. Simulation evaluations of an autonomous urban air mobility network management and separation service, in: 2018 Aviation Technology, Integration, and Operations Conference. Doi: 10.2514/6.2018-3365.

Brittain, M., Wei, P., 2018. Autonomous Aircraft Sequencing and Separation with Hierarchical Deep Reinforcement Learning. Icrat.

Cotton, W.B., 2019. Adaptive autonomous separation for UAM in mixed airspace. Integr. Commun. Navig. Surveill. Conf. ICNS 2019-April, 1–11. Doi: 10.1109/ICNSURV.2019.8735119.

Cui, M., 2013. Research on Method of Real-time Travel Time Collection Based on Simplified Road Network Model. Chongqing University.

Duan, H., 2005. Ant Colony Algorithms: Theory and Applications, Science Press.

EHANG216, n.d. EHANG216 Autonomous Aerial Vehicle Specs.pdf [WWW Document]. URL https://www.ehang.com/cn/ehangaav.

Federal Aviation Administration, 2016. Wake Turbulence Recategorization [WWW Document]. URL https://www.faa.gov/documentLibrary/%0Amedia/Order/JO_7110_123_(2).pdf.

German, B.J., Daskilewicz, M.J., Hamilton, T.K., Warren, M.M., 2018. Cargo delivery by passenger eVTOL aircraft: A case study in the san francisco bay area. AIAA Aerospace Sciences Meeting 2018, 1–13. https://doi.org/10.2514/6.2018-2006.

Hao, E., 2017. Research on Rerouting Tactics in Terminal Area Based on Task Complexity of ATC. Nanjing University of Aeronautics and Astronautics.

Hao, S., 2019. Research on Distributed Optimal Control Strategy of Urban Road Traffic System. Shandong University.

Kleinbekman, I.C., Mitici, M., Wei, P., 2020. Rolling-horizon electric vertical takeoff and landing arrival scheduling for on-demand urban air mobility. J. Aerosp. Inf. Syst. 17 (3), 150–159. https://doi.org/10.2514/1.I010776.

Kleinbekman, I.C., Mitici, M.A., Wei, P., 2018. eVTOL arrival sequencing and scheduling for on-demand urban air mobility. AIAA/IEEE Digit. Avion. Syst. Conf. - Proc. 2018-Septe, 1–7. Doi: 10.1109/DASC.2018.8569645.

Le, T., Kovács, P., Walton, N., Vu, H.L., Andrew, L.L.H., Hoogendoorn, S.S.P., 2015. Decentralized signal control for urban road networks. Transp. Res. Part C Emerg. Technol. 58, 431–450. https://doi.org/10.1016/j.trc.2014.11.009.

Li, C., Qu, W., Li, Y., Huang, L., Wei, P., 2020. Overview on traffic management of urban air mobility(UAM) with eVTOL aircraft. J. Traffic Transp. Eng. 20.

Littell, J.D., 2019. Challenges in vehicle safety and occupant protection for autonomous electric vertical take-off and landing (Evtol) vehicles. AIAA Propuls. Energy Forum Expo. 2019 https://doi.org/10.2514/6.2019-4504.

Luo, Y., Zhu, T., Wan, S., Zhang, S., Li, K., 2016. Optimal charging scheduling for large-scale EV (electric vehicle) deployment based on the interaction of the smart-grid and intelligent-transport systems. Energy 97, 359–368. https://doi.org/10.1016/j.energy.2015.12.140.

Ma, D., Xiao, J., Ma, X., 2020. A decentralized model predictive traffic signal control method with fixed phase sequence for urban networks. J. Intell. Transp. Syst Technol. Planning, Oper. 25 (5), 455–468. https://doi.org/10.1080/15472450.2020.1734801.

Mohamed Salleh, M.F. Bin, Tan, D.Y., Koh, C.H., Low, K.H., 2017. Preliminary concept of operations (ConOps) for traffic management of unmanned aircraft systems (TM-UAS) in urban environment, in: AIAA Information Systems-AIAA Infotech @ Aerospace. p. 0223. Doi: 10.2514/6.2017-0223.

Mohammed Salleh, M.F. Bin, Chi, W., Wang, Z., Huang, S., Tan, D.Y., Huang, T., Low, K.H., 2018. Preliminary concept of adaptive urban airspace management for unmanned aircraft operations, in: AIAA Information Systems-AIAA Infotech @ Aerospace. p. 2260. Doi: 10.2514/6.2018-2260.

Mueller, E., 2019. Enabling Airspace Integration for High Density Urban Air Mobility.

Pradeep, P., 2019. Arrival Management for eVTOL Aircraft in On-Demand Urban Air Mobility. Grad. Theses Diss.

Pradeep, P., Wei, P., 2018. Energy efficient arrival with rta constraint for urban evtol operations. AIAA Aerosp. Sci. Meet. 2018, 1–13. https://doi.org/10.2514/6.2018-2008.

Prevot, T., Rios, J., Kopardekar, P., Robinson III, J.E., Johnson, M., Jung, J., 2016. UAS Traffic Management (UTM) Concept of Operations to Safely Enable Low Altitude Flight Operations. Doi: 10.2514/6.2016-3292.

Shao, Q., Shao, M., Bin, Y., Zhu, P., Zhou, Y., 2020. Flight Recovery Method of Regional Multiairport Based on Risk Control Model. Math. Probl. Eng. 2020, 1–18. https://doi.org/10.1155/2020/7105381.

Sunil, E., Hoekstra, J., Ellerbroek, J., Bussink, F., Vidosavljevic, A., Delahaye, D., Aalmoes, R., 2016. The Influence of Traffic Structure on Airspace Capacity. Proc. 7th Int. Conf. Res. Air Transp.

Sun, Q., 2020. Research on airspace capacity assessment for airport terminal area. Civil Aviation University of China.

Tassiulas, L., Ephremides, A., 1992. Stability Properties of Constrained Queueing Systems and Scheduling Policies for Maximum Throughput in Multihop Radio Networks. IEEE Trans. Automat. Contr. 37, 1936–1948. https://doi.org/10.1109/9.182479.

Thipphavong, D.P., Apaza, R.D., Barmore, B.E., Battiste, V., Belcastro, C.M., Burian, B.K., Dao, Q. V., Feary, M.S., Go, S., Goodrich, K.H., Homola, J.R., Idris, H.R., Kopardekar, P.H., Lachter, J.B., Neogi, N.A., Ng, H.K., Oseguera-Lohr, R.M., Patterson, M.D., Verma, S.A., 2018. Urban air mobility airspace integration concepts and considerations, in: 2018 Aviation Technology, Integration, and Operations Conference. Doi: 10.2514/6.2018-3676.

Varaiya, P., 2013a. The Max-Pressure Controller for Arbitrary Networks of Signalized Intersections. Adv. Dynam. Netw. Model. Complex Transport. Syst. 163–192. https://doi.org/10.1007/978-1-4614-6243-9.

Varaiya, P., 2013b. Max pressure control of a network of signalized intersections. Transp. Res. Part C Emerg. Technol. 36, 177–195. https://doi.org/10.1016/j.trc.2013.08.014.
Vascik, P.D., Hansman, R.J., 2018. Scaling constraints for urban air mobility operations: Air traffic control, ground infrastructure, and noise. 2018 Aviat. Technol. Integr. Oper. Conf. 1–25 https://doi.org/10.2514/6.2018-3849.
Vidosavljevic, A., Delahaye, D., Sunil, E., Bussink, F., Hoekstra, J., 2015. Complexity Analysis of the Concepts of Urban Airspace Design for METROPOLIS Project. EIWAC 2015, 4th ENRI Int. Work. ATM/CNS.
Vincent, M.J., Trujillo, A.C., Jack, D.P., Hoffler, K., Tsakpinis, D., 2018. A recommended daa well-clear definition for the terminal environment. 2018 Aviat. Technol. Integr. Oper. Conf. https://doi.org/10.2514/6.2018-2873.
Wang, S., Huang, W., Lu, Z., 2006. Deduction of link performance function and its regression analysis. J. Highw. Transp. Res. Dev. 23, 107–110.
Wang, Y., Wang, Q., Wang, H., Jin, H., Dai, G., 2004. A Real-Time Scheduling Algorithm Based on Priority Table and Its Implementation. J. Sofw. 15, 358–368. https://doi.org/10.1023/B:APIN.0000033637.51909.04.
Wen, X., Huo, J., 2020. Research Based on Dynamic Priority for a Multi-runway Mixed Arrival-Departure Aircraft Scheduling Problem. Ind. Eng. Manag. 1–15.
Wongpiromsarn, T., Uthaicharoenpong, T., Wang, Y., Frazzoli, E., Wang, D., 2012. Distributed traffic signal control for maximum network throughput. IEEE Conf. Intell. Transp. Syst. Proceedings, ITSC 588–595. Doi: 10.1109/ITSC.2012.6338817.
Wu, Y., Sun, L., Qu, X., 2016. A sequencing model for a team of aircraft landing on the carrier. Aerosp. Sci. Technol. 54, 72–87. https://doi.org/10.1016/j.ast.2016.04.007.
Xu, Y., Zhang, H., Yang, L., Liao, Z., 2015. Analysis of Air Traffic Flow Characteristics in Airport Terminal Area Based on Observed Data. J. Transport. Syst. Eng. Inf. Technol. 15 (1), 205–211. https://doi.org/10.16097/j.cnki.1009-6744.2015.01.032.
Yang, X., Deng, L., Wei, P., 2019. Multi-Agent Autonomous On-Demand Free Flight Operations in Urban Air Mobility 1–13. Doi: 10.2514/6.2019-3520.
Zhang, J., Yang, W., 2018. The Optimization Based on Priority for a Mixed Arrival-Departure Aircraft Sequencing Problem. Oper. Res. Manag. Sci. 27, 115–121.
Zhang, J.F., Ge, T.T., Zheng, Z.X., 2017. Collaborative Arrival and Departure Sequencing for Multi-airport Terminal Area. Jiaotong Yunshu Xitong Gongcheng Yu Xinxi/Journal Transp. Syst. Eng. Inf. Technol. 17, 197–204. https://doi.org/10.16097/j.cnki.1009-6744.2017.02.029.
Zhu, G., Wei, P., 2019. Pre-Departure Planning for Urban Air Mobility Flights with Dynamic Airspace Reservation. Doi: 10.2514/6.2019-3519.